Volume 21 | Number 42 | 14 November 2019 | Pages 23221–23766

PCCP

Physical Chemistry Chemical Physics

rsc.li/pccp

ISSN 1463-9076

ROYAL SOCIETY OF CHEMISTRY | Celebrating IYPT 2019

PERSPECTIVE

Nicolas Giovambattista, Thomas Loerting *et al.*

Glass polymorphism and liquid–liquid phase transition in aqueous solutions: experiments and computer simulations

PCCP

PERSPECTIVE

View Article Online
View Journal | View Issue

Cite this: *Phys. Chem. Chem. Phys.*, 2019, **21**, 23238

Glass polymorphism and liquid–liquid phase transition in aqueous solutions: experiments and computer simulations

Johannes Bachler,[a] Philip H. Handle,[a] Nicolas Giovambattista *[bc] and Thomas Loerting *[a]

One of the most intriguing anomalies of water is its ability to exist as distinct amorphous ice forms (glass polymorphism or polyamorphism). This resonates well with the possible first-order liquid–liquid phase transition (LLPT) in the supercooled state, where ice is the stable phase. In this Perspective, we review experiments and computer simulations that search for LLPT and polyamorphism in aqueous solutions containing salts and alcohols. Most studies on ionic solutes are devoted to NaCl and LiCl; studies on alcohols have mainly focused on glycerol. Less attention has been paid to protein solutions and hydrophobic solutes, even though they reveal promising avenues. While all solutions show polyamorphism and an LLPT only in dilute, sub-eutectic mixtures, there are differences regarding the nature of the transition. Isocompositional transitions for varying mole fractions are observed in alcohol but not in ionic solutions. This is because water can surround alcohol molecules either in a low- or high-density configuration whereas for ionic solutes, the water ion hydration shell is forced into high-density structures. Consequently, the polyamorphic transition and the LLPT are prevented near the ions, but take place in patches of water within the solutions. We highlight discrepancies and different interpretations within the experimental community as well as the key challenges that need consideration when comparing experiments and simulations. We point out where reinterpretation of past studies helps to draw a unified, consistent picture. In addition to the literature review, we provide original experimental results. A list of eleven open questions that need further consideration is identified.

Received 24th May 2019,
Accepted 1st July 2019

DOI: 10.1039/c9cp02953b

rsc.li/pccp

1 Introduction

"Water, water, everywhere; Ne any drop to drink" recalls the "ancyent marinere",† pointing towards the fact that, despite its abundance, water is almost always encountered as part of a solution, often concentrated enough to render it non-potable. Indeed, this reflects the fact that pure H_2O is a formidable solvent, able to host an array of solutes spanning atoms, ions, inorganic and organic molecules, proteins, and polymers. One of the first scientists to systematically study aqueous solutions experimentally was Hofmeister who categorized solutes according to their ability to stabilize or destabilize protein solutions,[3] establishing the so-called Hofmeister-series. Since his work, vast amounts of research have been devoted to the study of aqueous solutions, filling more than five volumes of Franks' water treatise.[4] With the advent of computers, numerical studies of aqueous solutions have become possible. Pioneering Monte-Carlo (MC) simulations were performed by Clementi *et al.* who studied aqueous LiF[5] using Hartree–Fock interaction potentials.[6–8] Nowadays, computational studies of aqueous solutions are not uncommon and involve sophisticated computational techniques, including *ab initio* Car–Parinello molecular dynamics (MD),[9,10] hybrid quantum mechanical/molecular mechanical (QM/MM) methods,[11,12] and the use of polarizable models.[13–15]

Most experimental and computational studies of aqueous solutions have been performed at ambient conditions. Relevant topics addressed in the past include the dynamics and structure of water in the solvation shell of different solutes,[5,10–12] the structure making and breaking abilities of solutes,[16,17] hydrophobic solvation,[18] and water-mediated interactions.[18,19] Recently, more complex systems have been studied, including solutes at interfaces,[20,21] and solutions at astrochemical conditions.[22,23] Interestingly, computational and experimental studies of aqueous solutions at low temperatures, close to the

[a] *Institute of Physical Chemistry, University of Innsbruck, A-6020 Innsbruck, Austria. E-mail: thomas.loerting@uibk.ac.at*
[b] *Brooklyn College of the City University of New York, Brooklyn, NY 11210, USA. E-mail: NGiovambattista@brooklyn.cuny.edu*
[c] *PhD Programs in Physics and Chemistry, the Graduate Center of the City University of New York, New York, NY 10016, USA*

† Depending on your cultural background you might know this line from ref. 1 or ref. 2.

crystallization (T_m) and/or glass transition temperature (T_g), are rather scarce with only a few studies focusing on the glass transition of some aqueous solutions at low pressures (see the review article of Angell[24] and references therein). Not surprisingly, the behavior of aqueous solutions in the supercooled liquid (*i.e.*, the liquid at $T < T_m$) or glass state ($T < T_g$), remains poorly understood. This lack of understanding is partially due to the fact that water exhibits glass polymorphism (polyamorphism) and may exist in more than one liquid state. Indeed, it is an open question under what conditions a given aqueous solution may exhibit polyamorphism and/or a liquid–liquid phase transition (LLPT) at low temperatures.

The aim of this perspective is to discuss recent experimental and computational studies of supercooled and glassy aqueous solutions with special emphasis on the possibility of an LLPT and polyamorphism. In order to achieve this goal, we briefly discuss the complex behavior of pure water in the liquid (Section 1.1) and glass state (Section 1.2) as well as general aspects of aqueous solutions (Section 1.3). These sections serve as a framework to understand the behavior of aqueous solutions containing salts (Section 2), simple alcohols (Section 3) and other solutes (Section 4).

1.1 Liquid water: anomalous properties and the liquid–liquid phase transition hypothesis

Water is a complex liquid with an extensive list of anomalous properties.[25] For example, the density of liquid water increases upon isobaric cooling at 1 bar and reaches a maximum at 4 °C.[26–28] At higher pressures, the temperature of maximal density (TMD) shifts to lower values. Interestingly, computer simulations also predict that water may exhibit a density minimum upon isobaric cooling.[29] Several hypotheses were put forward in order to explain the complex behavior of water, including the presence of ρ, c_p, and κ_T maxima/minima lines in the p–T plane. Among the most common scenarios are (i) Speedy's stability limit conjecture,[30] (ii) the singularity free scenario[31,32] and (iii) the liquid–liquid critical point (LLCP) scenario.[33] These theoretical scenarios have been discussed extensively in the past and we refer the interested reader to ref. 28 and 34–39 for a detailed discussion. For the purpose of this perspective, we will focus on the LLCP scenario.

The key features of this scenario are shown in the phase diagram of Fig. 1. The red line indicates, qualitatively, the temperatures at which water may exhibit a density maximum (solid line) and/or minimum (dashed line) at a given pressure. Besides density (ρ), there are other quantities, such as heat capacity (c_p) and isothermal compressibility (κ_T) that show a non-monotonic behavior[26,28] and may also exhibit a minimum and/or maximum upon isobaric cooling. The orange and green lines in Fig. 1 represent the temperatures at which $c_p(T)$ and $\kappa_T(T)$ reach a maximum (solid lines) or minimum (dashed lines) at a given pressure.

The LLCP scenario is based on classical computer simulations[33] of the rigid ST2 model of water.[40] In this scenario, water at low temperatures ($T < 230$ K) can exist in two different liquid states, a low-density (LDL) and a high-density liquid (HDL).

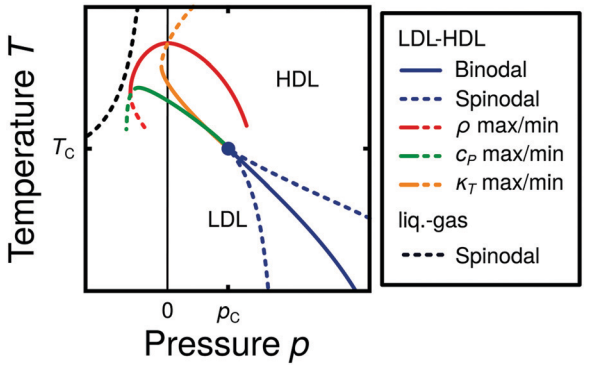

Fig. 1 Schematic phase diagram for water in the LLCP scenario (based on ref. 29). The blue circle is the LLCP and the blue lines show the associated LLPT binodal and spinodal lines. The maxima (solid lines) and minima (dashed lines) in density (red) and thermodynamic response functions, *i.e.*, isobaric heat capacity (green) and compressibility (orange), are also included. The dashed-black line represents the liquid–gas spinodal line.

As detailed in Fig. 1 LDL and HDL are separated by a first-order phase transition (binodal) line that ends at the LLCP. There, also the HDL → LDL and LDL → HDL spinodal lines are shown. Besides ST2 water which exhibits an unambiguous LLCP/LLPT,[29,41–46] indications for an LLCP were also reported for other rigid water models.[47–50] The estimated LLCP loci in different models are summarized in Table 1. Whether TIP4P/2005,[51] one of the most accurate water models,[52] exhibits an LLCP or not is currently under debate.[53–61] Most computational studies (including the ones listed in Table 1) are consistent with the existence of an LLCP in TIP4P/2005. However, in the case of some water models such as SPC/E and mW, an LLCP/LLPT is not accessible. For example, in SPC/E water[62] the LLCP is located below the

Table 1 LLCP temperature T_c, pressure p_c, and density ρ_c obtained from computer simulations of rigid water models. An estimation of the location of a possible LLCP based on experiments is also given

System	T_c/K	p_c/MPa	ρ_c/(g cm^{-3})	Source
		Unambiguous LLCP		
ST2[40]	246	186	0.94	Fig. 2 of ref. 29
	237 ± 4	167 ± 24	0.99 ± 0.02	Ref. 46
	247 ± 3	185 ± 15	0.96 ± 0.01	Fig. 1 of ref. 42
		LLCP located		
TIP4P[66]	190	150	1.06	Ref. 47
TIP4P-EW[67]	190	175	1.03	Ref. 50
TIP4P/2005[51]	193	135	1.012	Ref. 53
	182	170	1.017	Ref. 54 and 58
	182	158–162	1.02	Ref. 59
	175	175	0.997	Ref. 55
TIP5P[68]	217 ± 3	340 ± 20	1.13 ± 0.04	Ref. 49
TIP5P-E[69]	210	310	1.09	Ref. 48
		LLCP likely inaccessible ($T_c < T_K$)		
SPC/E[62]	130 ± 5	290 ± 30	1.10 ± 0.03	Ref. 63
	140–175	185–340	≈1.08	Ref. 64
		Experimental estimates		
H_2O	≈220	≈100	—	Ref. 70
H_2O	≈223	≈50	—	Ref. 71
D_2O	≈230 ± 5	≈50 ± 20	—	Ref. 72

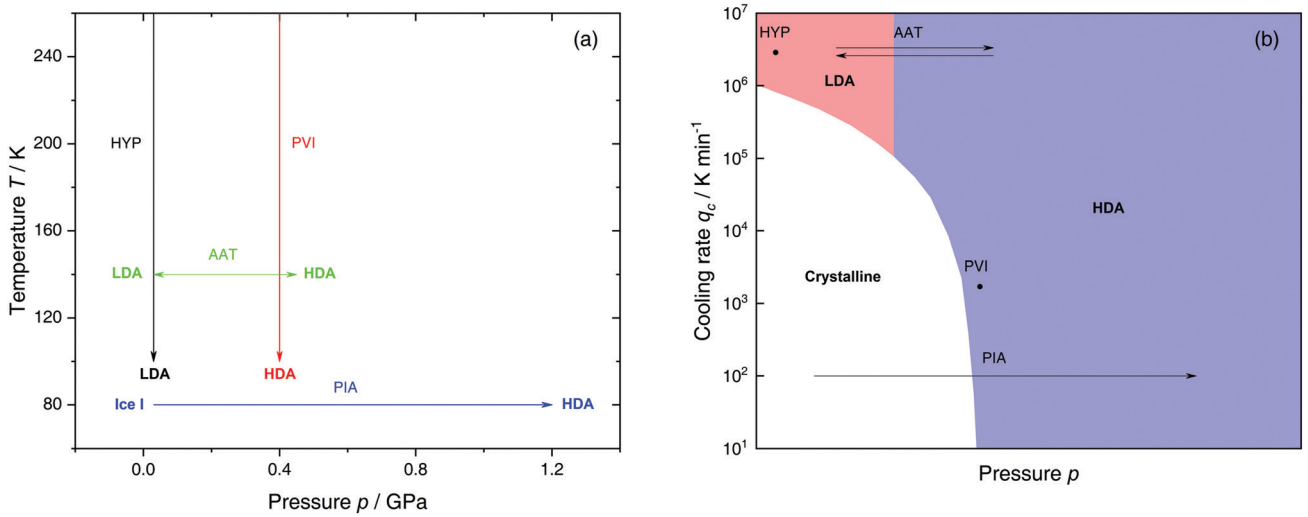

Fig. 2 (a) Experimental routes commonly followed to prepare glassy water, namely hyperquenching of liquid droplets (HYP),[89] pressure-vitrification of emulsified water (PVI),[113] pressure-induced amorphization of ice I (PIA)[109] and the first-order-like amorphous–amorphous transition (AAT).[91,92] (b) Schematic diagram indicating the final state of samples obtained after cooling liquid water to 80 K using different pressures p and cooling rates q_c. In addition, the constant temperature processes PIA and AAT from (a) are indicated by arrows. High-pressure crystalline states are ignored.

Kauzmann temperature (T_K),[63–65] at which the system is stuck in one basin of the potential energy landscape, thwarting any structural changes required for the transformation between LDL and HDL.

Interestingly, in this scenario the LLCP is directly connected with the presence of the ρ, c_p, and κ_T maxima/minima lines in liquid water (see Fig. 1). Indeed, close to the critical point, thermodynamic response functions can be expressed in terms of the correlation length and hence, they must form a single line at $T > T_c$ until they diverge at the LLCP.[29,36,73–78] This line in the p–T plane is referred to as the Widom line. Computer simulations of water and simple model liquids that exhibit an LLCP also show that the Widom line indicates (T, p) values where the dynamical properties of the liquid change profoundly.[78,79] Specifically, computer simulations show that water is a fragile liquid at temperatures above the Widom line. That is, the dynamic properties are non-Arrhenius and can be described, *e.g.*, by the empirical Vogel–Fulcher–Tammann equation.[80] At temperatures below the Widom line, however, it becomes a strong liquid (*i.e.*, the dynamic properties follow the Arrhenius equation). The occurrence of this fragile to strong dynamical crossover (FSDC) in supercooled water is consistent with experiments.[81–84]

1.2 Glass polymorphism in water

Confirming the phase diagram of Fig. 1 has been challenging for experimentalists. Very recent experiments on supercooled nanodroplets[85] and on supercooled stretched water[86] indeed suggest the presence of a maximum in κ_T at $-137 \leq p < 0.1$ MPa consistent with the possibility of an LLCP at positive p. We note however, that the significance of the results presented in ref. 85 is currently under debate.[87,88] The direct experimental investigation of the LLCP hypothesis in the supercooled liquid close to the suspected LLCP, has so far been hampered by rapid crystallization. This has prompted many experimentalists to study water in the glass state, below the suspected T_c. If liquid water is subject to extremely fast isobaric cooling then crystallization can be avoided and water can be vitrified.[89] In the LLCP scenario, cooling of LDL at low pressures leads to a low-density amorphous (LDA) ice while cooling of HDL at high pressures leads to a high-density amorphous (HDA) ice. The LDL ↔ HDL first-order phase transition, when extended into the glass state, becomes a first-order-like transition between LDA and HDA. Indeed, in the LLCP scenario, the experimentally observed LDA → HDA and HDA → LDA transformations correspond, respectively, to crossing the extensions of the LDL → HDL and HDL → LDL spinodal lines into the glass state.[90–93]

Additional support for the LLCP scenario is provided by computational and experimental studies of the glass transition temperature of amorphous ice. These studies show that water has two distinct T_gs, one for LDA[94–100] and one for HDA.[83,101–104] This strongly suggests that LDA and HDA are the glassy proxies of LDL and HDL, respectively (see ref. 105 and 106 for recent reviews on this topic). Winkel *et al.*[107] argue that the observed polyamorphic transition at 140 K takes place above both T_gs in the ultraviscous liquid domain of water. Further experimental support for the LLCP scenario stems from the behavior of isobars, showing slightly concave curvature at pressures exceeding 0.2 GPa.[71] This is expected for the LLCP scenario but not for the singularity-free scenario.[71] Furthermore, an apparent discontinuity in the melting lines of metastable high-pressure ices also speaks in favor of the LLCP hypothesis.[70,72] These results even allow for an estimation of the LLCP locus (see Table 1).

The most common routes to prepare LDA and HDA, followed in experiments and computer simulations are summarized in Fig. 2a. Specifically, the hyperquenching path HYP corresponds to ultrarapid cooling of liquid water at low pressure to produce LDA. Similarly, the pressure-vitrification path PVI involves cooling of liquid water at high pressure to produce HDA.

HDA can also be prepared by pressure-induced amorphization (path PIA) of ice I.[108,109] In addition, LDA and HDA can be interconverted by isothermal compression/decompression at $T \approx$ 125–140 K (amorphous–amorphous transition, path AAT).[28,92,93,110]

We note that the minimum cooling rates q_c necessary to prepare LDA/HDA from the liquid state (paths HYP and PVI in Fig. 2a) are strongly dependent on pressure. This is schematically shown in Fig. 2b. At ambient pressure, water is a bad glass former and crystallizes rapidly. Thus, the preparation of LDA requires hyperquenching, *i.e.*, very high cooling rates ($q_c > 10^6$–10^7 K min^{-1}).[89,111,112] By contrast, cooling the liquid at, *e.g.*, $q_c = 10^2$ K min^{-1} results in ice I. At $p = 0.4$ GPa, crystallization is easier to avoid and HDA can be prepared by cooling the liquid at $q_c \approx 10^3$ K min^{-1} (path PVI).[113]

Computational studies exploring the possibility of an LLPT and polyamorphism in aqueous solutions are almost exclusively performed using classical simulations with rigid molecular models. In this kind of computer simulations, crystallization events are very rare, an advantage relative to experiments. However, the limited time scales available in MD simulations, and computational power in the case of computer simulations in general, makes it challenging to directly access the LLPT in water, since the equilibration time increases dramatically at low temperature. That is, the system is glassy on the time scales probed in computer simulations at $T \approx T_c$ (an exception is the ST2 water model). For this reason, computational studies have also been used to study these non-equilibrium systems in simulations, as is done in experiments on amorphous ices. Here, computer simulations typically employ compression and/or cooling rates that are several orders of magnitude larger than the ones accessible in experiments.[114–118] As shown in Fig. 2a, at these rates experiments show that indeed, isobaric cooling yields either LDA or HDA. Anyhow, a direct comparison of non-equilibrium simulations and non-equilibrium experiments is difficult, since the phenomenology of glassy systems depends on the rates studied and as discussed, they differ by orders of magnitude in the two cases. This is reflected through the standard units for q_c being K ns^{-1} in MD simulations and K min^{-1} in experiments. Only recently the q_c employed in simulations comes close to the highest cooling rates reached in hyperquenching experiments.[119]

1.3 Aqueous solutions

The properties of aqueous binary solutions are, as for the case of pure water, very sensitive to pressure and temperature. For glassy solutions, the preparation process also plays a fundamental role. For example, a solution may crystallize/vitrify partly or fully upon isobaric cooling, depending on q_c and p. In addition, a systematic study of binary aqueous solutions needs to include the role of solute concentration. Specifically, the number of water molecules relative to the number of solute molecules determines the phase behavior and solution properties. Thus, it is reasonable to use the mole fraction x or, alternatively, the molar ratio R as concentration units. The mole fraction is defined as the number of moles of solute divided by the total amount of moles in mixture (pure water: $x = 0$) whereas R represents the ratio of water molecules to solute molecules (pure water: $R = \infty$). Note that for solutes which dissociate in aqueous solution, *e.g.*, NaCl, the R value can be specified either per individual ion (Na^+, Cl^-) or whole species ($NaCl_{aq}$). In this work we choose R to be the number of water molecules per number of ion pairs (*e.g.*, a NaCl–water solution with $R = 5$ consists of 1 NaCl per 5 H_2O molecules).

In aqueous solutions, the equilibrium liquid is stabilized with respect to ice I. That is, T_m is lowered, increasing the accessible T window. A remarkable natural example of this phenomenon is the Don Juan Pond located in Antarctica. This pond has such a large salt concentration that it refuses to freeze even at the harsh Antarctic conditions.[120] In fact, the solution making up the pond freezes around −50 °C.[120,121] This example illustrates that it is fairly easy to study cold aqueous solutions. Hence, one may conclude, erroneously, that it is possible to access the LLCP in water by adding some sort of solute, such as salt. However, extrapolating the properties of aqueous solutions to $x \to 0$ (pure water) has proven to be quite difficult as water steadily loses its anomalous properties with increasing solute concentration.[122–124] As a consequence, experimentalists have focused on the study of dilute solutions in the glass and/or highly-viscous liquid state, at concentrations where crystallization can be suppressed (although not entirely eliminated). The ultimate goal is to learn how solutions behave as a function of x and then, if possible, extrapolate the results to the case of $x = 0$ (pure water).

2 Solutions of salt in water

Experimental studies of liquid and glass polymorphism in salty aqueous solutions have mainly focused on LiCl, while computational studies concentrate on NaCl. This makes a direct comparison between experiments and computer simulations rather difficult. Hence, we discuss the experimental studies on LiCl–H_2O solutions in Section 2.1 and results from computational studies based on NaCl–H_2O solutions in Section 2.2. In Section 2.3 we briefly present research on aqueous systems containing other salts, *e.g.* bromides, nitrates, perchlorates and the ionic liquid hydrazinium trifluoroacetate.

2.1 LiCl–H_2O

Solutions of LiCl are the most studied binary aqueous systems in experiments. Many articles (*e.g.*, ref. 125–129 and references therein) show the equilibrium phase diagram composed of four different LiCl hydrates with the eutectic between ice and LiCl·5H_2O located at $x \approx 0.12$ ($R = 7.1$).[128] Strictly speaking this phase diagram is valid only for infinitely long (*i.e.*, equilibrium) experiments. In reality, even for rather slow cooling experiments these hydrates do not form. The variables that determine the states formed are q_c, p, x and T. Fig. 3 focuses on the states observed at liquid nitrogen temperature ($T = 77$ K), where the dependence on q_c and x at ambient pressure is outlined in Fig. 3a and on q_c and p for dilute solutions in Fig. 3b. Sections 2.1.1 and 2.1.2 describe experimental findings on the phase behavior of cooling at ambient and high pressure, respectively.

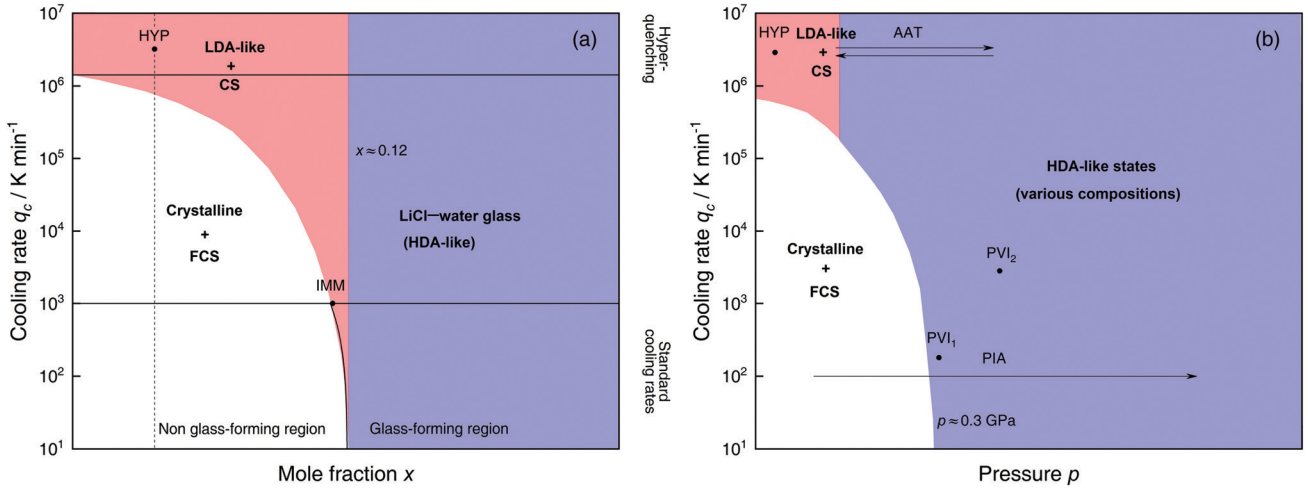

Fig. 3 Schematic diagrams indicating the final state of samples obtained after cooling LiCl–water solutions to 77 K using different mole fractions x, pressures p and cooling rates q_c. (a) Effect of q_c on solutions with different mole fraction x cooled at 1 bar. (b) Effect of q_c on dilute solutions ($x \approx 0.05$, dashed line in (a)) cooled at different pressures p. In addition, the constant temperature processes PIA and AAT are indicated by arrows. For clarity high pressure crystalline states are neglected. The white regions correspond to mixtures of ice I and freeze-concentrated glassy solution (FCS, $0.12 < x < 0.14$). Red (or blue) regions indicate non-crystalline solutions with water in an LDA-like (or HDA-like) state. FCS and CS are characterized as HDA-like containing significant amounts of salts. Points and arrows represent experiments: ref. 130 and 131 for HYP, ref. 126 for IMM, ref. 129 for PIA, original data from the present work for AAT, ref. 132 for PVI_1 and ref. 133 and 134 for PVI_2.

Sections 2.1.3 and 2.1.4 focus on transitions encountered by these non-equilibrium systems, namely pressure-induced amorphization (PIA) and the polyamorphic transition (AAT), respectively.

2.1.1 Isobaric cooling at low pressure. Inspecting Fig. 3a, it is immediately evident that the phase behavior of LiCl–water solutions quenched at low pressure changes drastically with increasing x, in particular, at the eutectic composition ($x = 0.12$). Specifically, solutions around and above the eutectic composition tend to supercool and vitrify easily, delineating the blue region in Fig. 3a.[127] At these concentrations, ice formation is avoided even for slow cooling rates ($q_c \approx 10$ K min^{-1}) yielding a rather homogeneous glass. In terms of structure the state of water in the solution corresponds to pure amorphous water either in the HDA or VHDA (very-high density amorphous ice) state, as deduced from Raman spectroscopy[135] and neutron scattering experiments.[136] VHDA represents the third polyamorph of water, forming at high-pressure conditions (>1 GPa).[137]

At $x < 0.12$ ice crystallization speeds up appreciably. Thus, solutions below the eutectic composition experience competition between crystallization and vitrification. At $x < 0.09$ ($R > 10$, white area in Fig. 3a) ice formation is unavoidable using standard cooling rates ($q_c \leq 10^3$ K min^{-1}) that can easily be reached in laboratories, *e.g.*, by plunging the sample into liquid nitrogen.[127] These cooling rates are employed to distinguish the glass-forming region (blue and parts of the red area in Fig. 3a) from the non-glass forming region (white area).[24] Consequently, in the non-glass forming region ice crystals begin to segregate while the water content in the remaining supercooled solution decreases, lowering the melting point of ice. For instance, for $x = 0.05$ and $q_c = 100$ K min^{-1} ice crystallization increases solute concentration in the remaining liquid, until the melting line of ice intersects with the glass transition line, typically at $0.12 < x < 0.14$ ($7.1 > R > 6$)[129] and $T \approx 137$ K. Below this temperature freeze-concentration comes to a stop, the freeze-concentrated solution is reached and vitrifies upon further cooling. Ultimately, a solid mixture of pure hexagonal ice and glassy patches of freeze-concentrated LiCl–H_2O solution (FCS) arises.

However, as nicely exposed in the early study by Angell and Sare[126] the behavior of LiCl–H_2O is even more complex. Rather than a crystalline substance also a second liquid may segregate from the parental liquid upon cooling (red area in Fig. 3a). In their work, aqueous LiCl solutions of $x = 0.09$ ($R = 10$) are quenched at $q_c \approx 10^3$ K min^{-1} [127] to 77 K at ambient pressure (liquid–liquid immiscibility point IMM in Fig. 3a). Instead of forming a homogeneous glass the LiCl solution separates into two distinct parts, a water-rich and a salt-rich glass. Accordingly, the mixtures obtained in the red segment are composed of water-rich amorphous solids, reminiscent of LDA, and concentrated solution (CS, with $x \approx 0.12$–0.14, just like the FCS).[126] Angell and Sare further showed that upon heating, the water-rich LDA-like state crystallizes while the CS simply exhibits a glass transition. This purported immiscibility of two liquids with different concentrations in LiCl–water solutions sparked considerable interest in the field and its consequences are still a topic of debate.[126,127,132,138–143]

The only way to avoid ice formation for dilute solutions $x < 0.09$ ($R > 10$) is the use of hyperquenching[89,111,112] ($q_c > 10^6$ K min^{-1}). Yet, at these high rates, the LiCl–water solutions appear to still phase-separate into water-rich domains and CS. Phase separation is inferred from Raman spectra of vitrified solutions for $x = 0.005$–0.091 ($R = 200$–10), which can be expressed as linear combination of the scans of pure LDA and (vitrified) LiCl–H_2O solution of $x = 0.14$ ($R = 6$).[131] Because of the presence of LDA domains this region is depicted in red in Fig. 3a, including the small red segment (IMM) studied by

Angell and Sare.[126] The rapid phase segregation upon hyperquenching is striking as it implies that LiCl is barely soluble in LDA. This low solubility is consistent with the numerical simulations of Corradini *et al.* on the NaCl–H_2O system (see Section 2.2).[47,144–148]

The phase separation into two non-crystalline parts described above has been observed in the glass state. Similar findings have also been obtained in the supercooled liquid state. Such a liquid–liquid separation in LiCl aqueous solutions was reported using neutron scattering methods. Specifically, using transient grating experiments, Bove *et al.*[149] showed the onset of phase segregation at T = 190 K, in solutions of LiCl–water for $x < 0.14$ ($R > 6$). Below T = 190 K, the homogeneous solution separates into domains of concentrated solution and short-lived nanometer-sized water-rich domains. This represents the high-temperature analogue of observations in the hyperquenched states. However, it still remains unclear whether phase separation in salty solutions relates to the LDA–HDA separation in pure water or is simply a separation into two distinct solutions of different concentration.

2.1.2 Isobaric cooling at high pressure. Fig. 3b details the non-equilibrium states reached by cooling a pressurized solution of $x \approx 0.05$ at various rates. The figure is based on several experimental studies[132–135,150–152] whereas numerical studies have not been done in this context. On first sight, it becomes clear that Fig. 3a and b resemble each other very much, even though the former plots the states in dependence of x and the latter in dependence of p. This testifies that electro-restrictive forces of ions and external pressure have similar effects.[153] Other than the cooling experiments at ambient pressure described in Section 2.1.1 most isobaric cooling experiments were done in the pressure range 0.2–0.5 GPa (points PVI_1 and PVI_2 in Fig. 3b). Pioneer work on vitrified pressurized dilute LiCl–H_2O solutions was undertaken by Kanno[132] who used a specialized high-pressure differential thermal analysis (DTA) apparatus developed by Angell and co-workers.[154] Kanno quenched LiCl solutions of $x \approx 0.05$ (R = 20) at p = 0.25 GPa and $q_c \approx 180$ K min^{-1}. The nature of the samples was assessed based on heating experiments. When heating the solution at ambient pressure the DTA scan is similar to the scan of pure water (see bottom curve in Fig. 4), displaying two exothermic peaks. In fact, the location of the first exotherm at 1 bar is very close to the one reported by Amann-Winkel *et al.* for the transformation of pure HDA to LDA.[83] Thus, we assign the low-T peak to the transition of water within the solution, from HDA to LDA, while the high-T peak signals cold-crystallization of LDA to ice I. In this context, cold-crystallization is defined as a crystallization event of a supercooled liquid or amorphous solid that occurs upon heating, but has not occurred in the previous cooling run of the liquid. Even though Kanno was not aware of the similarity of his scan and the one of HDA[83] this finding clearly shows that the high-pressure quenched sample contains HDA and is thus located in the blue region in Fig. 3b (PVI_1). The appearance of HDA is also supported by the observation that cooling pure water at similar pressure (0.3 GPa) leads to HDA, not LDA.[113] Furthermore, Suzuki and Mishima[134] confirm the presence of HDA based on Raman and differential scanning calorimetry (DSC) on pressure-vitrified aqueous LiCl solutions with $x < 0.10$ recorded at ambient pressure.

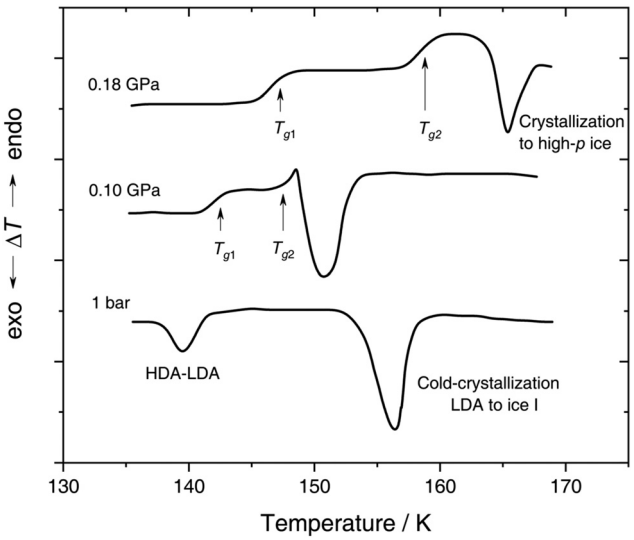

Fig. 4 *In situ* DTA scans of $x \approx 0.05$ (R = 20) LiCl–H_2O solution vitrified at 0.25 GPa with $q_c \approx 180$ K min^{-1}, then reheated at various pressures with a scanning rate of 8 K min^{-1}. The figure is adapted from ref. 132.

With increasing pressure, two distinct glass transitions gradually appear in the DTA scans (marked by arrows in Fig. 4). The double glass transition at p = 0.18 GPa is strong evidence that the solution is exhibiting liquid–liquid immiscibility during the isobaric cooling process and hence, is composed of two phase-separated glasses, one of which resembles pure HDA. By contrast solutions quenched at ambient pressure[126,131] (*cf.* Section 2.1.1) contain pure LDA as one of the two separated glasses. The first glass transition $T_{g,1}$ marked by an arrow in Fig. 4 matches the glass transition temperature of pure HDA at 0.10 and 0.18 GPa (reported to be 140 ± 5 K and 145 ± 5 K, respectively[106]) very well. The second T_g observed by Kanno (see Fig. 4) at ≈155 K and 0.18 GPa pertains to the pressurized CS which does not crystallize. Please note that Kanno[132] originally interpreted the double glass transition differently: the first T_g was assigned to the near-eutectic solution and the second T_g to a water-rich component, without taking HDA-like states into consideration.

Additional evidence that isobaric quenching of LiCl–water solutions at high pressures leads to phase-separation into a water-rich HDA state and a salt-rich HDA-like state is provided in ref. 133. Here, dilute LiCl–water solutions (x = 0.021–0.091, $R \approx$ 10–50) were cooled under pressure (p = 0.5 GPa) at $q_c \approx 10^4$ K min^{-1} (PVI_2, Fig. 3b), and resulting vitrified aqueous solutions were characterized using Raman spectroscopy. Remarkably, for more concentrated solutions, the Raman scans can be expressed as linear combinations of the Raman spectra of pure HDA and the spectra of highly-concentrated LiCl–water solutions. The segregation into water-rich and concentrated solution naturally becomes more pronounced with increasing mole fraction of LiCl. Due to the spectral similarity of concentrated (HDA-like) solution and pure HDA it remains unclear if HDA is free from dissolved LiCl.[133]

2.1.3 Pressure-induced amorphization (PIA). The possibility to reach high-density amorphous states by pressurizing ice I at 77 K has been known since 1984.[109] However, for frozen salt solutions this route was not studied until 30 years later when Ruiz *et al.*[129] prepared glasses by PIA of crystallized LiCl–water solutions. For this reason the study provides a new perspective on the ambiguities presented above. PIA of LiCl–H_2O solutions can be studied at $x < 0.12$ (eutectic point) since the phase behavior of the solution at higher concentrations is dominated by the salt and ice formation does not occur with $q_c = 15$ K min^{-1} (see Fig. 3a).[155] However, upon slowly cooling solutions with $x < 0.12$ at ambient pressure patches of ice crystals precipitate, trapping FCS in between them. At low temperatures the FCS vitrifies, producing a LiCl–H_2O glass of near-eutectic composition threading through the network of ice crystals. It is unclear whether this mixed crystalline/glassy sample homogenizes upon pressurization or stays segregated. Ruiz *et al.*[129] find that the hexagonal ice in the mixture exhibits pressure-induced amorphization just like pure water while the FCS mainly acts as a spectator. As a result, the sample is not homogeneous after PIA but contains two HDA-like solids: one that is rather pure, forming *via* ice I, the other containing salt.

For samples quench-recovered to 1 bar, X-ray analysis and low temperature DSC scans closely resemble the ones from pure water HDA samples. Signs for FCS are seen in the DSC scans in the form of a weak glass transition. Interestingly, the latent heat of the HDA → LDA transition per mole of water stays constant, even when the salt fraction is increased. This implies that not only the pure ice patches but also the water bound in FCS undergoes a transition upon heating at ambient pressure at the polyamorphic transition. The state attained after this transition cannot be pure LDA because it never cold-crystallizes upon further heating. Ruiz *et al.*[129] suggest that this state is of low-density with significant amounts of salt embedded. By contrast, previous publications conclude that hydration water is forced into the HDA structure through the influence of ions even at ambient pressure.[134–136,156] These apparently conflicting interpretations might be reconciled in different ways: (i) the polyamorphic transition occurs in the FCS part of the sample yet does not result in LDA but an LDA-like state of increased density; (ii) the transition in the FCS is not polyamorphic but continuous, slowly releasing enthalpy upon heating; and/or (iii) the transition is associated with water molecules being expelled from the salty solution, leaving behind a glassy solution of $x = 0.14$ (LiCl·6H_2O) containing all the unfreezable water.

To distinguish between these scenarios currently not enough information is available and further experiments are required, *e.g.*, annealing of PIA samples below the polyamorphic transition would allow to exclude either (i) or (ii).

2.1.4 Polyamorphism in LiCl–H_2O solutions

Proposed p–T–x state diagram. Fig. 5 shows a *p–T–x* diagram suggested by Suzuki and Mishima[134] detailing the polyamorphism in LiCl–H_2O (assuming ice formation can be avoided). The diagram is similar to a combination of Fig. 3a and b but leaving out the cooling rate dependence. Hence, it is valid for the comparatively long time scale given by $q_c \approx$ 20–40 K min^{-1}.[134] Here, the *p–T* plane (at $x = 0$, *cf.* Fig. 1) is the well-known non-crystalline state diagram of water based on the LLPT hypothesis (assuming ice formation is avoided). Similarly, the *T–x* plane (at $p = 0$), corresponds to the (non-crystalline) state diagram of binary LiCl–H_2O solutions at 1 bar. As described in the previous sections, cooling of LiCl–water solutions may lead to phase separation even without crystallization (indicated as the red immiscibility region). The most intriguing feature in Fig. 5 is the presence of an immiscibility dome connecting the ambient pressure immiscibility (colored in red) to the LLPT line in pure water (dashed lines). To explain the dome let us envision a solution at $x = 0.05$ pressure-vitrified at $p = 0.3$ GPa: Suzuki and Mishima[134] regard such samples to be rather homogeneous, composed of LiCl dissolved in HDA (HDA–LiCl). Upon isothermal decompression at 130 K the dome is entered just below ≈0.2 GPa where almost salt-free LDA segregates from the HDA–LiCl.[151,152] The involved separation resembles the polyamorphic HDA → LDA transition in pure water supplemented by changes in salt concentration. Parts of the solvent water transform from an HDL-like to an almost pure LDL-like state (path AAT in Fig. 3b). By contrast, decompression above 150 K leads to crystallization (not covered in the non-crystalline state diagram shown in Fig. 5). Thus, the proposed critical point at the apex of the dome (red point in Fig. 5) is not accessible in these experiments because it is preempted by crystallization. Note that crystallization to ice I only appears after the HDA → LDA AAT upon decompression.[151,152] In other words LDA/LDL is found to be the mother of ice, as nicely phrased by Bullock and Molinero.[157] This is also consistent with the findings of Bove *et al.*[149] where nanophase segregation into water-rich clusters of low density and salt-rich solution occurs upon decreasing temperature after which ice I can grow.

A different state diagram emerges when inspecting the work by Kanno,[132] particularly as presented here in Fig. 4. According to Kanno[132] liquid–liquid immiscibility is even found for PVI samples. That is, additional states would need to be present in the state diagram. This means that Fig. 5 might represent a simplification of a more complex scenario, where also HDA-like states show separation into almost pure HDA and CS (HDA-like structure). Upon decompression at 130 K (from 0.3 GPa), both domains need to be considered individually. In the water-rich segments of the sample HDA transforms to LDA just like in pure water whereas the salt-rich CS is hardly affected. It remains an open question which of the two scenarios is closest to reality, specifically, whether the transition to pure LDA upon decompression originates from pure HDA or HDA–LiCl.

Glass transition temperatures. One may now wonder whether the co-existing states are liquid or glassy at 140–150 K. This query requires knowledge of all three glass transition temperatures, namely for LDL, pure HDL (or HDL–LiCl) and near-eutectic CS. The glass transition temperature of CS ($x = 0.12$, $R = 7.1$) is ≈136 K at 1 bar,[127] similar to T_g of pure water.[83] T_g(CS) barely depends on the initial concentration of solute[127] (see also T_g line in Fig. 5). For $x = 0.048$ T_g(HDL) is estimated to be around 140 K at 0.1 GPa,[101,152] compared with T_g(LDL) ≈ 130 K at 1 bar.[130,158] All these T_gs are very close to the temperature range employed in Mishima's decompression experiments[151,152] and vary by a

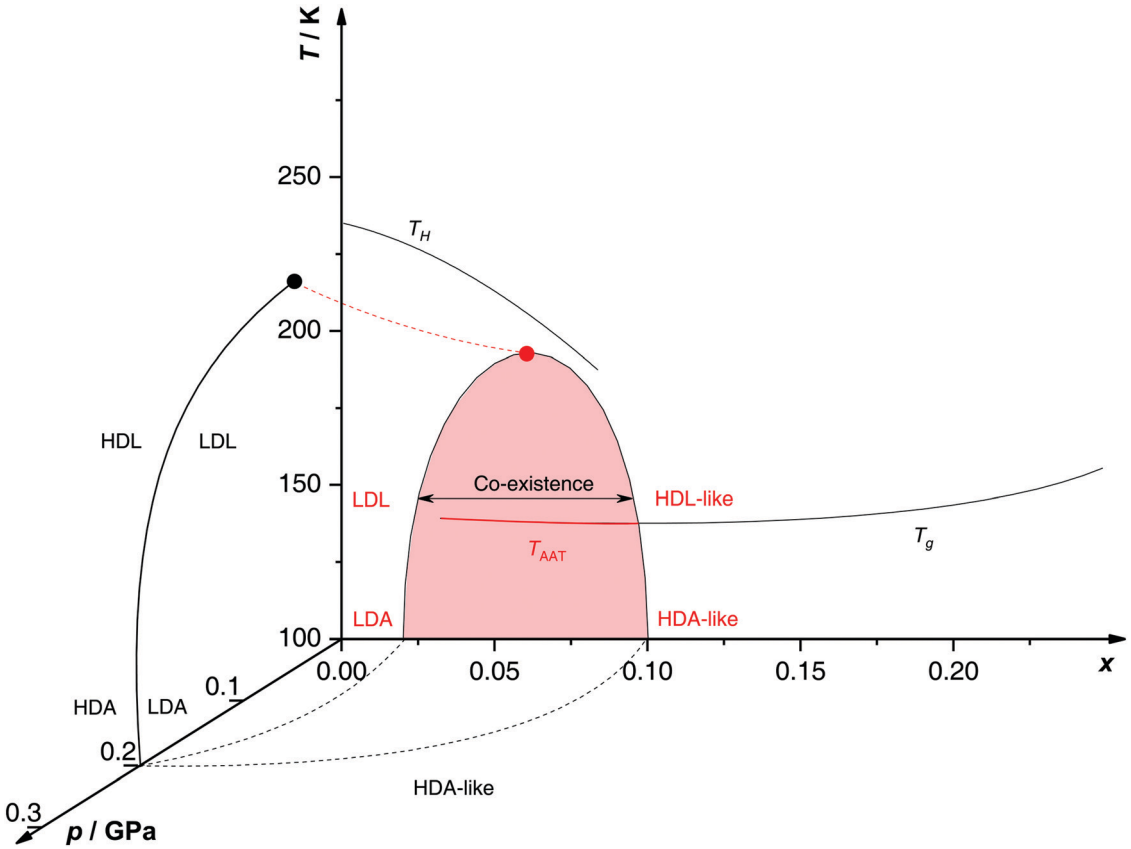

Fig. 5 Non-crystalline state diagram of LiCl–H_2O adapted from ref. 134. The dome (red: T–x plane at ambient pressure, black dashed lines: p–x plane at 100 K) separates regions in which solvent water appears as HDA- or LDA-like. This immiscibility dome appears as the LLPT line in the p–T plane where the red dashed line indicates a smooth connection. Additionally, the homogeneous nucleation temperature of emulsified solutions T_H, the T_g line of homogeneously vitrified solutions and the amorphous–amorphous transition line T_{AAT} from HDA-like to pure LDA are shown. Please note that this picture might be an oversimplification (see text).

few degrees depending on concentration, pressure and time scale of experiment. Consequently, it is not clear whether the transformations occur in the liquid, glass or mixed liquid–glass state. In the mixed case several scenarios are possible, namely (i) HDA expels pure LDL, (ii) HDL expels LDA which turns into LDL upon further decompression and (iii) HDL expels LDA which remains LDA. The latter is excluded based on the findings by Giovambattista *et al.*[159] who show that T_g of LDA decreases with increasing pressure. Whether LDA or LDL is expelled depends most importantly on the time scale of the experiment, and whether HDA or HDL is present at the onset of the transition additionally depends on the choice of salt concentration.

Up to today it remains contested how the salt influences the T_g of the LDA-type states, where the type of preparation determines the outcome. For hyperquenched LDA samples T_g for dilute solutions ($x < 0.09$, $R > 10$) shows complex behavior involving a minimum and maximum as a function of x. This indicates an interplay of plasticization and anti-plasticization of the hydrogen bonding network caused by ions.[127] In contrast such behavior is not observed for LDA samples prepared starting from hexagonal ice.[158] This indicates that the distribution of ions is different in the different types of LDA samples. Possibly, there is not enough time for the ions to be expelled from LDA in the hyperquenching experiment (leading to a supersaturated amorphous state), whereas there is ample time for samples prepared based on slow procedures. Also for pressure-vitrified samples two distinct scenarios have been discussed: Kanno[132] regards them as two immiscible solids whereas Mishima and Suzuki[101,133,134,151,152] rather convey them to be homogeneous, namely LiCl dissolved in HDA (HDA–LiCl). HDA–LiCl shows the glass transition temperature as depicted by the black T_g line in Fig. 5.[127] Once T_g intersects with the co-existence dome the homogeneous solution spontaneously decomposes according to HDA–LiCl → LDA + CS. That is, the glass transition line develops into phase segregation where the driving force is the insolubility of ions in the LDA matrix.[131,151,152,160]

This finding is corroborated by investigation of the melting line of ice IV under pressure.[161] The solubility of salt in solution can be assessed based on the melting point depression. A sudden melting point depression is observed in case of melting ice IV to HDL–LiCl above 0.1 GPa, conforming that LiCl is soluble in HDL/HDA. By contrast no such depression is found when ice IV melts to LDL below 0.1 GPa. This immediately suggests that the salt dissolved in HDL is responsible for the depression whereas LDL is immiscible with LiCl. The change in

melting behavior upon variation of pressure locates the LLPT line near 0.1 GPa in LiCl–H_2O.

Reversibility of the LDA ↔ HDA transition. The work of Mishima[151,152] is based on decompression experiments of glassy solutions vitrified under pressure. However, compression/decompression cycles probing the reversibility of the transformation between HDA ↔ LDA transformation in LiCl–water solutions have not been reported. Such experiments were performed for the case of water at T = 130–140 K.[91] Since LiCl tends to suppress the formation of ice, a natural question is whether the reversible LDA ↔ HDA transformation in LiCl–water solutions can be observed at $T > 140$ K. Extending Mishima's work we here report new experiments on compression/decompression cycles probing for the reversible HDA ↔ LDA polyamorphism. Our pressure-cycling experiments might answer the question whether the phase separation is driven by water or the salt. In the former case the phase segregation indicates polyamorphism akin to pure water whereas in the latter case the dome is unrelated with an LLPT in a single component. Furthermore, the presence of the salt might raise the crystallization temperature of the amorphous samples allowing for measurements extended to higher temperatures in the non-crystalline state.

Specifically, we follow a similar protocol to the one used by Mishima[91] to investigate polyamorphism (LDA ↔ HDA). Volume curves for both pure water and an x = 0.04 LiCl–water solution are shown in Fig. 6. The main point of Fig. 6 is the abrupt volume change at $p \approx 0.45$ GPa during the compression of both pure water and the LiCl–water solution which signals the LDA → HDA first-order-like transition. During decompression, HDA transforms back to LDA at $p \approx 0.05$ GPa, *i.e.*, there is hysteresis between the up- and downstroke transition. The similarity between the pure water and LiCl–water curves in Fig. 6 immediately reinforces the notion that the dome in Fig. 5 is caused by polyamorphism in water. Just like in neat water (black curve) both the stepwise volume increase during compression (LDA → HDA) and stepwise decrease during decompression (HDA → LDA) are also observed for LiCl–H_2O (red curve).

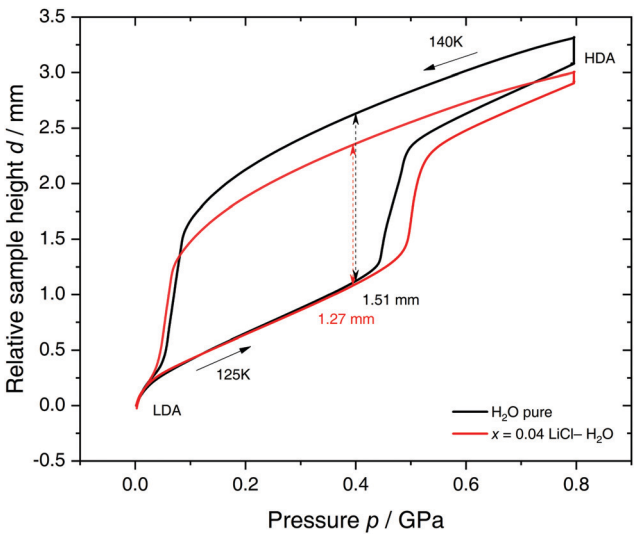

Fig. 6 Reversible cycling between low- and high-density amorphous water states in pure water (black) and in x = 0.04 LiCl–H_2O solution (red). Densification is indicated as double-headed arrow. 300 μL of solution were slow quenched ($q_c \approx$ 10–100 K min^{-1}) at 1 bar to 80 K, compressed isothermally at 80 K (PIA in Fig. 3b) and annealed following the protocol of Winkel *et al.*[93] In the next step the HDA/LiCl sample was decompressed at 140 K and recompressed at 125 K (path AAT in Fig. 3b) following the protocol of Loerting *et al.*[164]

The double-arrows in Fig. 6 indicate the volume change during the transformation. Adding salt to water (x = 0.04) has the effect of reducing the volume change during the transformation, relative to the case of pure water, *i.e.*, changes in the sample height (d) are 1.51 and 1.27 mm for pure water and the LiCl–water solution, respectively. This leads to a reduction in volume change of (1.51–1.27)/1.51 × 100% ≈ 16% indicating that there are less water molecules in the solution that participate in the LDA ↔ HDA transition. We note, however, that if one assumes that (i) the glassy solution is composed of water domains and domains of LiCl–H_2O FCS (x = 0.12–0.14, $R \approx$ 7.1–6), and that (ii) the water molecules in the FCS domains do not participate in the polyamorphic transition, then the volume change in the glassy solution should be ≈28%, relative to the case of pure water. The fact that the volume change during the transition decreases by only ≈16% with addition of salt, leads us to believe that the FCS solution also densifies during compression, which is consistent with the work of Suzuki and Mishima.[162] In other words, the reversible polyamorphic transition seems to take place between pure LDA and HDA while near-eutectic LiCl–H_2O patches simply densify continuously. Perhaps, even slow mixing of FCS with HDA might be the case. This conclusion is supported by our additional experiments (not shown here) at higher decompression temperatures. Just like in pure water raising the temperature from 140 to 142 K results in crystallization of HDA to ice IX.[163] That is, the salt does not help to extend the polyamorphic transition to higher temperatures, which reinforces that the polyamorphic transition takes place in pure water patches, with the salty patches acting as spectator only. The same conclusion was given as a conjecture by Mishima[152] who observed that the transition pressure of HDA → LDA remains unaffected by the addition of salt (which is corroborated in Fig. 6).

Polyamorphism at higher pressures: HDA ↔ VHDA? In pure water besides LDA and HDA polyamorphism also HDA and VHDA polyamorphism is debated vividly.[28,137] VHDA can be interconverted reversibly with HDA *via* different thermodynamic paths.[110,137] The HDA ↔ VHDA transition is not well understood and it has been speculated that this continuous transformation can be due to a (third) critical point in water buried deep in the glassy state.[165]

Relevant to this work, we note that HDA–VHDA polyamorphism was also probed in LiCl–water by Bove *et al.* at near-eutectic concentrations (x = 0.14, R = 6) utilizing neutron scattering as well as computer simulations.[136] The experiments indicate a reversible transition from HDA–LiCl to VHDA–LiCl involving a very small density change. This finding was confirmed by both *ab initio* and classical MD simulations. According to the

simulations the transition is associated with an increase of the coordination number of Li^+ from 4.25 in HDA–LiCl to 5.25 in VHDA–LiCl. Interestingly, it was found that the underlying molecular-level mechanism involves one water molecule moving into the first hydration shell of the Li^+ ions during the compression process and not a Cl^- ion. However, this pressure-induced transformation is ten times broader than in pure water,[164] covering a p-interval of $\approx$1.5 GPa. For comparison, MD simulations of pure water during the LDA $\rightarrow$ HDA transformation at similar conditions show that the glass–glass transformation expands over a p-range of only 0.1–0.3 GPa[115,117] or even less.[166,167] The smoothness and small density change in the HDA–LiCl $\rightarrow$ VHDA–LiCl transformation, relative to the LDA $\rightarrow$ HDA first-order like transition in pure water, supports the view where the reported glass–glass transformation in LiCl aqueous solutions with R = 6 is not related to the LLPT between LDL and HDL in pure water. For a solution of R = 6 one may expect only $\approx$1–2 water molecules between ions, assuming that the solution is homogeneous and no phase separation occurs. At such high concentrations, it is not possible to distinguish a hydration layer surrounding the ions separated by bulk-like water domains. That is, the movement of one water molecule from the second hydration shell to the first that characterizes HDA–VHDA polyamorphism is not possible. If the goal of studying water glass polymorphism with salts is to suppress ice formation while maintaining, somehow, the glass–glass transformations of bulk water, then much smaller concentrations (such as x = 0.04 used for the study of LDA $\leftrightarrow$ HDA polyamorphism in Fig. 6) are required.

Paraphrasing, the experiments by Bove *et al.*[136] are driven by changes in the distribution of ions but unrelated to water polyamorphism. Similar conclusions apply to the study of Suzuki and Mishima[162] on vitrified solutions of x = 0.11. That glass polymorphism is not necessarily related to an LLPT at higher temperatures is also found in computer simulations of some water models, such as SPC/E, where a smooth LDA $\rightarrow$ HDA transformation is observed[114,159] but an LLCP/LLPT, if it exists, may be located deep in the glassy state.[63–65] In addition, we note that the relationship between glass and liquid polymorphism can depend on additional factors such as the preparation process of the starting glass (see, *e.g.*, ref. 90, 116, 118, 168 and references therein).

2.2 NaCl–H_2O

In a series of publications, Corradini and collaborators[47,144–148,169] studied the phase behavior of NaCl–water solutions in the liquid state, over a wide range of T and p using MD simulations. Four (dilute) solutions are considered, x = 0, 0.0119 (R = 250/3), 0.0240 (244/6) and 0.0364 (R = 238/9), covering for instance the typical salt concentration in seawater ($x \approx 0.0098$).[47] In all cases, the MD simulations are performed using the TIP4P water model.[66] The main focus of these studies is to search for the existence of an LLCP in NaCl solutions. Corradini *et al.*[47] estimate that, for pure TIP4P water, an LLCP exists at p_c = 150 MPa, T_c = 190 K and ρ_c = 1.06 g cm^{-3}. In particular, as shown schematically in Fig. 7, they find that the LLCP shifts towards lower p and higher T as x increases. Interestingly, the LLCP is located at negative pressures in all solutions studied and, at the highest concentration, the LLCP is very close to the liquid $\rightarrow$ vapor spinodal line. In addition, increasing x has the effect of shrinking the LDL–HDL co-existence region (area between spinodal (dashed) lines in Fig. 7), expanding the HDL stability region towards low pressures while shrinking the LDL domain.[47,144] It follows that adding NaCl to TIP4P water stabilizes HDL at low p and T, which is consistent with experiments on LiCl–water solutions.[135,136,151,152,170] From a molecular point of view, the addition of NaCl to water was found to barely influence the water–water radial distribution functions. The small effects of adding salt to water that were detectable in the average structure of the solutions resemble the effect of increasing the external pressure on pure water.[145]

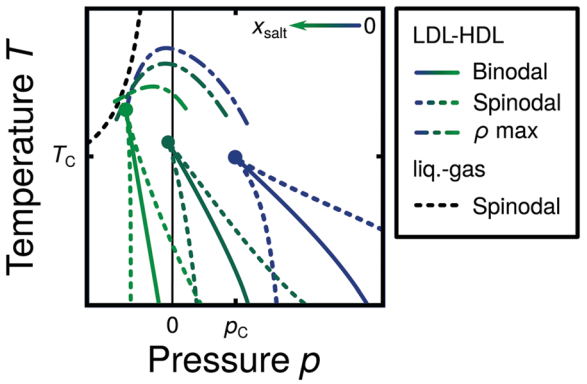

Fig. 7 Schematic diagram based on MD simulations[144] illustrating the effects of increasing the salt concentration on NaCl–water solutions (x increases from blue to green color). In the case of pure water, the LLCP is located at p_c and T_c (blue lines). Adding NaCl shifts the LLPT and LLCP into the negative pressure domain and shrinks the LDL–HDL co-existence region between the two spinodals. At sufficiently large concentrations, the LLCP is expected to move below the liquid–gas spinodal lines, effectively vanishing.

We note that the LLCP in (pure) TIP4P water reported in these studies occurs at very low temperatures, in the supercooled liquid regime,[47] where equilibration times can become relatively large. In this regard, the computer simulations of ref. 47, 144, 146, 148 and 169 are rather short ($<$40–50 ns) and hence, longer MD simulations may be necessary in order to directly confirm the existence of an LLCP in TIP4P water as well as in the associated NaCl aqueous solutions. Nonetheless, there is strong evidence in ref. 47, 144, 146, 148 and 169 at higher temperatures, *i.e.*, in the equilibrium liquid state, that supports the results summarized in Fig. 7. Specifically, as shown in Fig. 1, if the LLCP shifts towards lower p and higher T, one would expect a similar shift in the lines of κ_T, c_V and c_p maxima with increasing x. After all, at low temperatures, all these supercritical lines must meet at the Widom which connects to the LLCP. Although not necessary, one may also expect a similar shift in the TMD line as concentration increases. Corradini *et al.* show that, indeed, at all concentrations studied, the κ_T and c_V maxima meet at low temperatures in the p–T plane close to the estimated LLCP.[47,144,146,148,169] Similarly, the TMD line shifts towards lower p and T, as x increases (see Fig. 7).[144,146]

The MD simulations of NaCl aqueous solutions also show an FSDC when the system crosses the c_V-maxima line upon isochoric cooling at low pressures.[148] This is important because an FSDC has been found in water models such as ST2 and TIP5P[78] that also exhibit an LLCP (see Table 1). The available data suggest that the FSDC in the studied NaCl aqueous solutions also shifts towards lower p and larger T with increasing x, as one would expect from Fig. 7.[148]

We note that the MD results for the NaCl solutions are in agreement with the experiments of Archer and Carter[122] on NaCl–water solutions with $x \leq 0.0975$ ($R = 9.3$), at ambient pressure and $T \geq 202$ K. Specifically, it was found that the TMD line can be observed only up to $x \approx 0.0348$ ($R = 28$). At $x > 0.0348$ crystallization interferes. The simulations show that both the TMD and c_p maxima lines shift towards lower T as the salt concentration increases. Similar results were also found by Holzmann *et al.*[171] who studied the effect of x and p on the behavior of NaCl–water solutions *via* MD simulations of TIP4P-Ew water. They also find that increasing x and/or p shift the TMD line towards lower T. We would like to note, however, that from the experimental perspective, the presence of an FSDC in salt–water solutions is still under extensive debate.[172–180]

An independent study of NaCl–water solutions related to the presence of liquid polymorphism in aqueous solutions was performed by Longinotti *et al.*[181] In this work, replica exchange MD simulations of NaCl–water solutions are presented for $p = 0.1$ MPa, in a T-range corresponding to the equilibrium and supercooled liquid. Concentrations are limited to low values, $x = 0.00343$ ($R = 872/3$), 0.0115 ($R = 858/10$), 0.0233 ($R = 838/20$). These MD simulations employ the TIP5P-E water model[182] for which the LLCP is accessible to equilibrium simulations and is well-characterized. The LLCP in this model is located at $p_c = 310$ MPa, $T_c = 210$ K and $\rho_c = 1.09$ g cm^{-3}.[48] In addition, the ion force field employed in this work is specifically designed for TIP5P-E water.[183] Longinotti *et al.* focus on the effects of x on the TMD line, c_p-maxima line, and the FSDC at $p = 0.1$ MPa (*cf.* Fig. 1). They observe that, consistent with the work of Corradini *et al.*,[144,146] all these supercritical lines shift towards lower T (at $p = 0.1$ MPa) with increasing amounts of NaCl. Interestingly, the results of Longinotti *et al.* are different from the picture provided in ref. 144 where the (TIP4P) LLCP moves to negative pressures with increasing x. If the LLCP in solutions of TIP5P-E water and NaCl was also located at negative pressures, cooling the solution at normal pressure should lead to a HDL → LDL phase transition upon cooling. Instead, Longinotti *et al.*[181] only find a c_p-maxima line which is inconsistent with the presence of an LLCP at $p < 0$.

The above named differences could very well be the result of the different force fields used. Indeed, one of the main challenges in classical computer simulations is the unknown sensitivity of the results to the force fields employed. It follows that results from classical computer simulations have to be taken with caution. Even in the case of pure water, different water models that show liquid polymorphism may exhibit the LLCP at different p and T (see Table 1). In the case of ion–water solutions, the force field chosen to represent the ion–ion and ion–water interactions provide additional complexity.[184,185] For example, in the case of KCl–water solutions, different ion force fields can induce ion aggregates in biomolecular systems independently of the water model.[186] In the case of LiCl–water solutions, Aragones *et al.*[187] show that simple modification in the treatment of the ion–ion short-range interactions (*i.e.*, Lennard-Jones) can lead to large improvement in the structure of the salt–water solution relative to experiments and even influence the tendency of ions to cluster (phase separate). For the case of TIP4P NaCl–water solutions, Corradini *et al.*[146] compared results obtained in TIP4P water and NaCl employing two different force field for the ions and found that their MD simulation results are not sensitive to the ion force field.

A different approach to study the effect of salt on polyamorphism of water was used by Biddle *et al.*[188] By performing theoretical calculations starting from the two-state thermodynamics model for pure water[189] they found that increasing NaCl concentration significantly decreases the critical pressure while having barely an effect on the critical temperature.[188] The LLPT model by Biddle *et al.*[188] fits the experimental c_p data of Archer and Carter[122] on NaCl–H_2O solutions well. This demonstrates that the measured behavior of c_p is consistent with the occurrence of a LLPT.[188]

2.3 Other salt solutions

Glassy aqueous solutions of salts other than LiCl and NaCl have been studied intensely in experiments. Yet, these studies do not address the possibility that the corresponding solutions exhibit polyamorphism and/or an LLPT. Instead, homogeneous nucleation temperatures and glass transition temperatures are usually measured. As for the case of LiCl–water solutions, crystallization is common in dilute solutions at ambient pressure and standard cooling rates ($q_c \leq 10^3$ K min^{-1}, see Fig. 3a). Only for high salt content these solutions can easily reach the glass state (glass-forming region).[24] Angell and co-workers determined the glass-forming region for various chloride,[127] nitrate[127,190] and acetate solutions.[191] For none of the salts, very dilute amorphous solutions were accessed. Additionally, they measured the homogeneous nucleation temperature T_H in emulsified aqueous alkali halide solutions as a function of pressure.[192,193] Compared to pure water, T_H of ice is in general lower for salty solutions where the smaller ions have the largest effect.[194] This is because smaller ions exert larger electro-restrictive forces and a higher pressure on the surrounding water molecules.

Glass transition temperatures were determined for hyperquenched dilute aqueous solutions, namely LiCl (see Section 2.1.1), LiI, NaCl, CsCl, $MgCl_2$, LiBr, KBr and tetra-*n*-butylammonium bromide.[195] Remarkably, T_g decreases on the initial addition of the solute, reaches a minimum value, and then increases again. This is rather unusual in glass physics since the simple case is characterized by the Gordon–Taylor equation not allowing for any extrema in T_g.[196] The location of the minimum is characteristic for each solute.[195] This indicates two competing effects: a loosening of the H-bond network thereby lowering T_g (''plasticization''), and an ''anti-plasticization'' which is believed to relate to H-bonding with solutes, hydration of ions and stability of ion pairs, causing an increase in T_g.[195] In this

context, vitrified dilute nitrate[197–201] and perchlorate[197,202] solutions show more direct contact between ions ("contact-ion pairs") whereas solvent-separated ion pairs are depleted compared to the liquid. The change of T_g(LDA) with changing x suggests that the ions are still contained in LDA for hyperquenched samples, possibly because the ions are kinetically trapped in an unstable state that would otherwise demix.

Non-ideal mixing suppresses water anomalies and hence, prevents a straightforward extrapolation of data obtained for solutions ($x > 0$) to the case of pure water ($x = 0$).[122–124] In recent work, however, Zhao and Angell[203] show that hydrazinium trifluoroacetate, a salt consisting of a weak-field cation and a simple anion, mixes almost ideally with water. In addition, they claim that crystallization is avoided in a rather concentrated solution ($x = 0.156$) during the cooling process with $q_c = 20$ K min^{-1}. The key finding is a sharp spike in heat capacity both on cooling and subsequent heating at ≈185 K and 1 bar which is interpreted as an LLPT. On the basis of the ion concentration employed, the authors estimate an effective pressure for water within the solution (at the observed LLPT) of 0.15–0.20 GPa.[204,205] This is consistent with recent calculations, locating the LLPT of pure water between 186 K and 198 K at p = 0.15–0.20 GPa.[39,189] Interestingly, with increasing solute concentration the heat capacity spike disappears, leaving behind a simple step in $c_p(T)$ as it is observed in common glass-forming aqueous solutions.[203] This change from LLPT to glass transition may be related to the switch from water- to salt-dominated behavior upon increase of concentration. Finally, this observation is consistent with experiments on pure water by Winkel *et al.*,[93,107] who suggest a decompression-induced LLPT at 0.076 GPa and 140 K.

The apparent first-order transition occurring in the hydrazinium trifluoroacetate aqueous solution was further probed using infrared studies and MD simulations.[206] Most importantly, upon supercooling at 1 bar a discontinuous shift of the OH-stretch band position to higher frequencies is observed at ≈190 K, as expected for a first order LLPT. The spectra of the high-temperature and low-temperature liquid are similar to pure LDA and HDA, respectively. Crystallized samples, however, exhibit a different IR pattern. Evidence based on diffraction that this LLPT is indeed between two liquids is missing, though. In the future, it would be interesting to check for the absence of, *e.g.*, crystalline hydrates based on diffraction experiments. Additionally, a systematic study of the purported LLPT as a function of pressure, *e.g.*, compression/decompression cycles similar to the ones done by Mishima[91] would improve our understanding for the relation of this transition to the LLPT in pure water. If the interpretation is correct one would expect c_p to show a broader and flatter maximum upon dilution, associated with the crossing of the Widom line, rather than a spike, associated with the LLCP. Yet, this remains open to be demonstrated.

3 Solutions of alcohols in water

3.1 Glycerol–H_2O

Glycerol ($C_3H_8O_3$) has a widespread application in many industries[207] including cosmetics, cryopreservation (*e.g.* ref. 208–211 and references therein), food[212] and even manufacturing of adhesives, synthetic plastics and explosives.[213] The ability to promote supercooling has also opened a vast field for fundamental science. Glycerol molecules compete with water for hydrogen bonds by effective integration into the H-bond network, ultimately leading to the suppression of water crystallization.[214] The detailed underlying processes still remain elusive up to the present day. However, much effort has been made to fully characterize the complex phase behavior of aqueous glycerol solutions. The equilibrium phase diagram is of the eutectic type where the eutectic composition of $x \approx 0.28$ ($R \approx 2.6$) freezes around 225 K.[215] By contrast to many salts glycerol (like glycerol-rich aqueous solutions) does neither form any hydrates nor crystallizes as a pure component. It is rather an excellent glass former with a $T_g \approx 190$ K. As for the case of LiCl–water, the behavior of glycerol–water solutions in the glass and supercooled liquid state is poorly understood, where states not shown in the equilibrium phase diagram are involved. Our discussion on glycerol–water follows closely the discussion of Section 2 for LiCl–water. In Section 3.1, we describe the glassy states attained in experiments upon cooling the solutions at low- (Section 3.1.1) and high-pressure (Section 3.1.2). The pressure-induced transformations PIA and AAT are discussed in Section 3.1.3. MD simulation studies on glycerol–water are collected in Section 3.1.4, and Section 3.2 comprises low temperature studies in alcohol–water solutions other than glycerol.

3.1.1 Isobaric cooling at low pressure

Glycerol-rich region: x = 0.38–1.00 (R = 1.6–0). In highly-concentrated glycerol–water solutions no signatures of polyamorphism and LLPT are found, in fact, the phase behavior and dynamics are relatively simple. Specifically, at all cooling rates the solutions can be vitrified without signs of ice formation (except when seeded). Broadband dielectric spectroscopy (BDS) studies on glycerol–water mixtures above $x = 0.60$ display only one main relaxation process.[216,217] The T-dependence of the corresponding relaxation times follows the Vogel–Fulcher–Tammann equation[80] (non-Arrhenius regime) indicating that the solutions are fragile (in the fragile/strong classification of liquids[24]). The maximally freeze-concentrated solution (MFCS), defined as the intersection of the $T_g(x)$ line and the extrapolated $T_m(x)$ line, has been found to be at $x = 0.38$ ($R = 1.6$).[215–224] At and below this concentration, there are enough water molecules available to form hydrogen bonds with every OH group of the glycerol molecules.[214]

Intermediate region: x ≈ 0.17–0.38 (R ≈ 4.9–1.6). At $0.17 \leq x \leq 0.38$ there are enough water molecules in the solution that allow for the formation of water domains at low temperatures.[217,225] Accordingly, in the case of very slow cooling rates ($q_c < 1$ K min^{-1}, beyond the range in q_c shown in Fig. 9a) these solutions phase-separate into ice and domains containing water and glycerol during the cooling process.[221,224] As soon as ice crystals start to precipitate the supercooled glycerol–water domains become more and more concentrated until the corresponding concentration reaches the MFCS of $x = 0.38$. This phase separation upon crystallization is also observed in more dilute solutions ($x < 0.17$). However, already moderate cooling rates (≈10 K min^{-1})

lead to full vitrification. Although phase separation can be prevented upon cooling, cold-crystallization becomes inevitable upon reheating. It was suggested that cold-crystallization of an $x \approx 0.20$ solution yields a novel two-dimensionally ordered structure of ice.[226–228] However, the existence of a new 2D ice phase is ambiguous because of the striking similarity to cubic ice.[228–230]

Since crystallization can still easily be avoided in glycerol–water solutions at $x \approx 0.17$–0.38, it is natural to ask whether these solutions can exhibit liquid and/or glass polymorphism at low temperatures. This question was addressed by Murata and Tanaka in ref. 229. They presented experimental evidence of an isocompositional LLPT without macroscopic phase separation in glycerol–water solutions with $x \approx 0.17$ which sparked particular interest in the field.[231,232] However, the evidence for such an LLPT in glycerol mixtures near these concentrations has been challenged. Murata and Tanaka interpret microscopy images upon cooling the liquid solution (liquid I) to show transformation into another liquid (liquid II) of the same composition. They observe two types of mechanisms, nucleation and growth of liquid II at 180 K or spinodal decomposition of liquid I at 173 K. Upon reheating, the two liquids were reported to exhibit different glass transition temperatures. Murata and Tanaka concede that liquid II contains nanometre-sized ice crystals which grow to macroscopic size only at temperatures as high as 205 K, *i.e.*, far above the observed LLPT. Based on Raman data of pure LDA and HDA at 30 K they suggest that liquid II is tetrahedrally ordered and thus relates to LDL of pure water whereas liquid I connects more to an HDL state. In both liquids glycerol molecules are mixed homogeneously with no sign of phase separation during the transition.

Soon after the experiments of Murata and Tanaka[229] other groups investigated glycerol–water solutions at low temperatures, searching for the purported LLPT. In particular, Suzuki and Mishima[230] focused on the "transformation of liquid I to II" using Raman spectroscopy. They pointed out that the conclusions by Murata and Tanaka mentioned above are questionable since it is "inappropriate that the 170 K-recorded Raman spectra are compared with the Raman spectra of two amorphous ices which are recorded at different temperature of ≈32 K". According to Suzuki and Mishima[230] the glycerol–H_2O glass of $x = 0.17$ rather resembles a state fluctuating between LDL and HDL, instead of a pure HDL state as proposed by Murata and Tanaka.[229] More specifically, Suzuki and Mishima[230] regard this state to be supercritical, above the LLCP at 150 K (see Section 3.1.2). This supercritical fluid converts to what appears to be cubic ice at 170 K after 30 minutes. In other words, Murata and Tanaka might have observed crystallization of glycerol–water, rather than an LLPT.

The latter view is backed by independent findings of Popov *et al.*[222] and Zhao *et al.*[223] In both works the LLPT was reassigned to crystallization, where the second glass transition relates to the MFCS ($x = 0.38$) but not to a liquid of the same composition $x = 0.17$. At $x = 0.17$ immediate crystal growth is avoided upon cooling with moderate rates, but formation of ice nuclei is not. When reheated, the glassy matrix containing the nuclei first devitrifies at $T_g \approx 160$ K, and subsequently the ice nuclei grow. This cold-crystallization causes the remaining glycerol–water solution to freeze-concentrate until the MFCS is reached. This MFCS shows a $T_g \approx 175$ K, and thus, explains the second glass transition observed by Murata and Tanaka near 170 K. It is not valid however, to view this composition change induced by cold-crystallization as an LLPT.

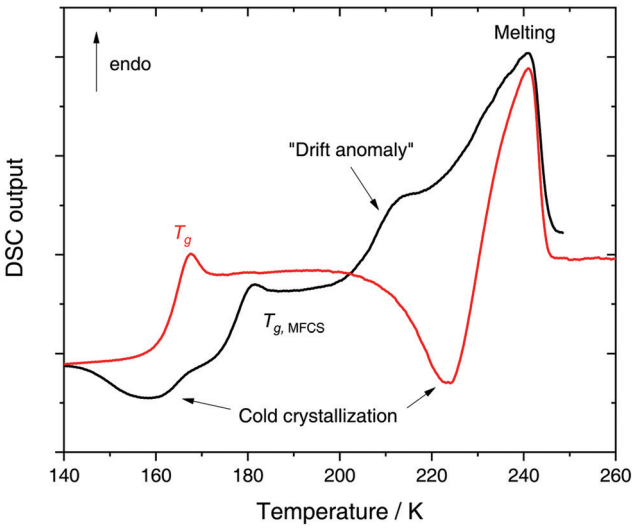

Fig. 8 DSC heating scan at 1 bar (30 K min^{-1}) of a glassy $x = 0.20$ glycerol solution vitrified at 30 K min^{-1} and ambient pressure (red curve) or produced by pressure-induced amorphization at 77 K (black curve).

In a recent work we performed detailed experiments on amorphous glycerol–water and also conclude that solutions at $x \geq 0.20$ do not exhibit polyamorphism.[224] To show this, we include in Fig. 8 (red curve) the DSC scan of a glycerol–water glassy solution of $x = 0.20$ at 1 bar. This DSC scan shows a glass transition at $T_g \approx 160$ K followed by cold-crystallization at ≈225 K. There are no signs of an HDA → LDA (AAT) exotherm before cold-crystallization intervenes. $T_g \approx 160$ K in Fig. 8 (red curve) implies a glycerol content somewhere in between $x = 0$ ($T_g = 136$ K)[105] and $x = 0.38$ ($T_{g,MFCS} = 175$ K, black curve). Furthermore, we find that samples with $x = 0.20$ quenched at ambient pressure to ≈80 K do not experience a sharp polyamorphic transformation upon isothermal compression (see also Section 3.1.3).[224] This is because the samples contain water that is already in an HDA-like state at ambient pressure as opposed to the LDA-like state proposed by Murata and Tanaka.[229] In the state diagram shown in Fig. 9a the solutions at $x = 0.17$ and 0.20 are, thus, located in the HDA-dominated domain (blue).

Despite these arguments doubting the existence of an LLPT in glycerol–water solutions with $x = 0.17$–0.20,[222–224,230] recent vibrational spectroscopy studies[233] initiated reconsideration along the lines of Murata and Tanaka.[229] Upon keeping liquid I for 100 min at 170 K the time-dependence of the transformation obeys the Avrami equation with an exponent $n = 2.9$. This is similar to the exponent reported for the purported LLPT in triphenyl phosphite ($n = 3$)[234] but different from the exponent associated with crystallization of the liquid at 195 K ($n = 1.7$)

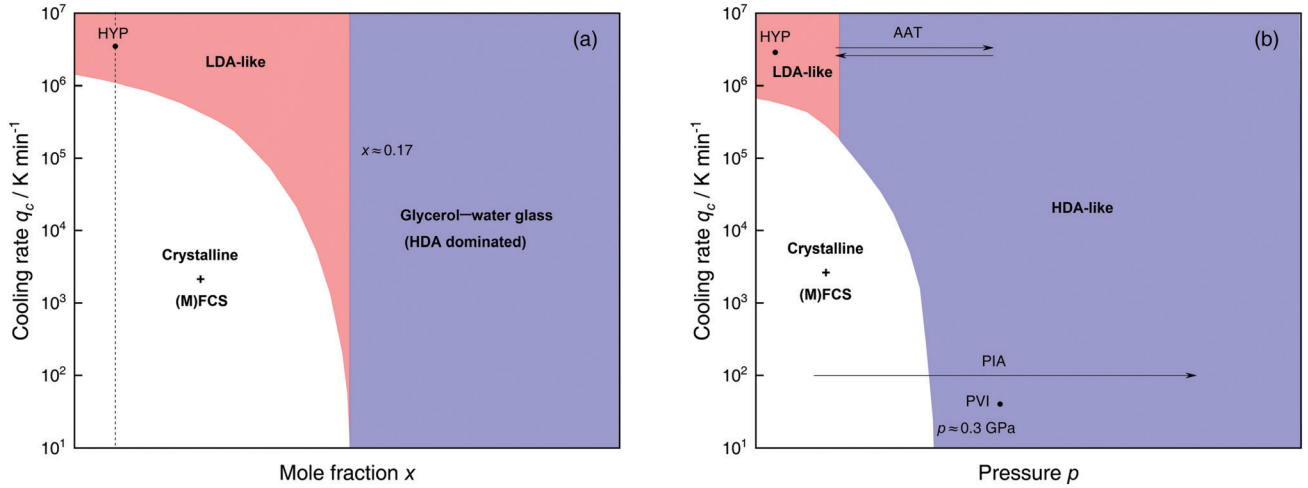

Fig. 9 Schematic diagrams indicating the final state of samples obtained after cooling glycerol–water solutions to 77 K using different mole fractions x, pressures p and cooling rates q_c. (a) Effect of q_c on solutions with different mole fraction x cooled at 1 bar. (b) Effects of q_c on dilute solutions ($x \approx 0.05$, dashed line in (a)) cooled at different pressures p. In addition, the constant temperature processes PIA and AAT are indicated by arrows. For clarity high pressure crystalline states are neglected. The white regions correspond to mixtures of ice I and (maximally) freeze-concentrated glassy solution ((M)FCS, $x \leq 0.38$). Red (or blue) regions indicate non-crystalline solutions with water in an LDA-like (or HDA-like) state. Points and arrows represent experiments: ref. 195 for HYP, ref. 224 for PIA, ref. 230 for PVI/AAT and original data in the present work for AAT.

and cold-crystallization of glassy water (n = 1.5 at <150 K‡). The exponents $n < 2$ were interpreted as nearly completed nucleation just before diffusion controlled growth of spherical particles.[236–238] However, an exponent $n = 3$ is also expected for interface-controlled cold-crystallization.§ That is, similarity of exponents alone is not a sufficient criterion to conclude whether the solution is evolving *via* an LLPT or precipitation of ice. In addition, it is not clear whether triphenyl phosphite indeed exhibits an LLPT or not (*e.g.*, formation of an inter-glacial phase[239–241]). In other words, the Avrami kinetics of a genuine LLPT is not known. In fact, the vibrational spectra above the alleged LLPT closely resemble the crystallized liquid, and so it still holds that the liquid–liquid transition was mistaken for crystallization of nanocrystals (small enough not to induce turbidity).

Water-rich region: $x \approx 0.00$–0.17 ($R = \infty$–4.9). As the glycerol mole fraction decreases below x = 0.17, crystallization becomes more and more favorable over vitrification (see white area in Fig. 9a).[216,217,222,225] Thus, most experiments in this concentration region focus on crystallized solutions.[216,217,221,222,224,225] The only technique known to avoid crystallization in dilute solutions is hyperquenching. In fact, we are only aware of the hyperquenching experiments by Hofer *et al.*[195] in which T_g was determined for glycerol–water (and other solutions) with x = 0–0.05. Interestingly, $T_g(x)$ for glycerol–water solutions exhibits a minimum as observed in the case of salty water.[195] This points to a homogeneous sample of LDA containing glycerol, just like in the case of hyperquenched LiCl solutions. By contrast to the case of LiCl the LDA–glycerol solution might be intrinsically stable, without the tendency to demix at higher temperature. In simulations vitrification can easily be achieved due to the accessible high cooling rates. This facilitates studies on glassy states of dilute glycerol–water as is elaborated in detail in Section 3.1.4.

Let us now move on from hyperquenched glassy solutions to partly crystallized glycerol–water solutions. Not surprisingly, they exhibit complex dynamics. Specifically, three main dielectric relaxation processes are observed as opposed to the single one in concentrated solutions ($x \geq 0.38$).[216,217,225] They are attributed to relaxation of (i) domains of pure hexagonal ice and (ii) MFCS, and to the (iii) so-called temperature-drift anomaly (see black line in Fig. 8).[217,221,225] The origin of the drift anomaly is still under debate, but it has been observed for all partly crystallized solutions below x = 0.38.[217,221,224,225] In DSC scans the drift anomaly appears above 200 K and overlaps with melting (see black curve in Fig. 8 for an example). Feldman and co-workers[216,217,222,225] explained the temperature-drift anomaly by proposing the formation of a layer of non-crystalline, interfacial water between ice and MFCS that constantly exchanges water molecules with its surroundings. Consequently, the observed feature was regarded as a second glass transition.[217,225] On the other hand, Inaba and Andersson[221] dismissed a second glass transition by pointing out that the resulting T_g would be unfeasibly high. Not even inclusions of pure glycerol ($T_g \approx 185$ K) could exhibit glass transitions at such high temperatures let alone pure water ($T_g \approx 136$ K). Instead, they suggested that the temperature-drift anomaly is due to ice formation through cold-crystallization immediately followed by ice melting, similar to observations made for sucrose–water.[242] In using optical microscopy Bogdan *et al.*[243] even observed simultaneous melting and cold-crystallization of citric acid solutions and explained this finding by the presence of two different freeze-concentrated solutions: the first one produced by microscopic cryo-concentration in between small crystals,

‡ We note that Bruijn *et al.*[233] cite Avrami exponents from Hage *et al.*[235] at 155 K while Hage *et al.* report the crystallization kinetics of HGW (LDA) below 150 K.
§ Avrami exponents in general depend on the type of experiment, *e.g.*, in surface sensitive techniques such as spectroscopy one dimension is lost, decreasing the exponent by one.

the second one produced by macroscopic cryo-concentration at the moving crystallization front. Thus, assuming similar behavior for glycerol–water the drift anomaly might be cold-crystallization of a more dilute freeze-concentrated solution, while a more concentrated one starts to melt.

3.1.2 Polyamorphism in samples produced by pressure-vitrification (PVI). The main advantage of studying glycerol–water solutions under pressure is that pressure tends to suppress the formation of ice, even for dilute solutions. Specifically, Fig. 9b shows the state of the solutions (glassy or crystalline) after isobaric cooling to 80 K at different p and q_c. Cooling the solution at p = 0.3 GPa a slow rate $q_c \approx 40$ K min^{-1} is sufficient to avoid crystallization for concentrations as low as x = 0.05 (path PVI). This provides a unique opportunity to explore polyamorphism in water-rich solutions of $x \leq 0.17$. Liquid and glass polymorphism in glycerol–water was studied in detail by Suzuki and Mishima for pressure-vitrified mixtures with x = 0.02–0.12.[230] Upon isothermal decompression of the so-prepared HDA-like mixtures, LDA-like states could be produced at p = 1 bar ($T \approx$ 140–150 K). In particular, they show that the LDA-like and HDA-like solutions can be reversibly transformed into one another by isothermal compression/decompression cycles, just as LDA and HDA in pure water.

By analyzing the hysteresis of the polyamorphic transition at different temperatures and concentrations, a co-existence region of high- and low-density glass states can be accessed (see red dome in Fig. 10). Suzuki and Mishima locate the LLCP in solution, at a given x, as the highest temperature of the co-existence region, *i.e.*, they define the LLCP as the point where the polyamorphic transition in the glycerol–water system disappears. For example, at $x \approx 0.135$, the LLCP is determined to be around $p \approx 0.045$ GPa and $T \approx 150$ K (red circle in Fig. 10).[230,244]

The existence of a two-phase region (red dome in Fig. 10) has already been proposed by Biddle *et al.*[188] (see Section 2.2) based on thermodynamic arguments about the LLPT. The main difference in the p–T–x state diagrams proposed for glycerol–water (Fig. 10) and LiCl–H_2O solutions (Fig. 5) is that, in the case of glycerol, there is no immiscibility dome at ambient pressure. Immiscibility occurs only at $p \approx$ 0.1–0.2 GPa. In other words, there is miscibility of glycerol, but immiscibility of LiCl with LDA-like solvent water states at low p.

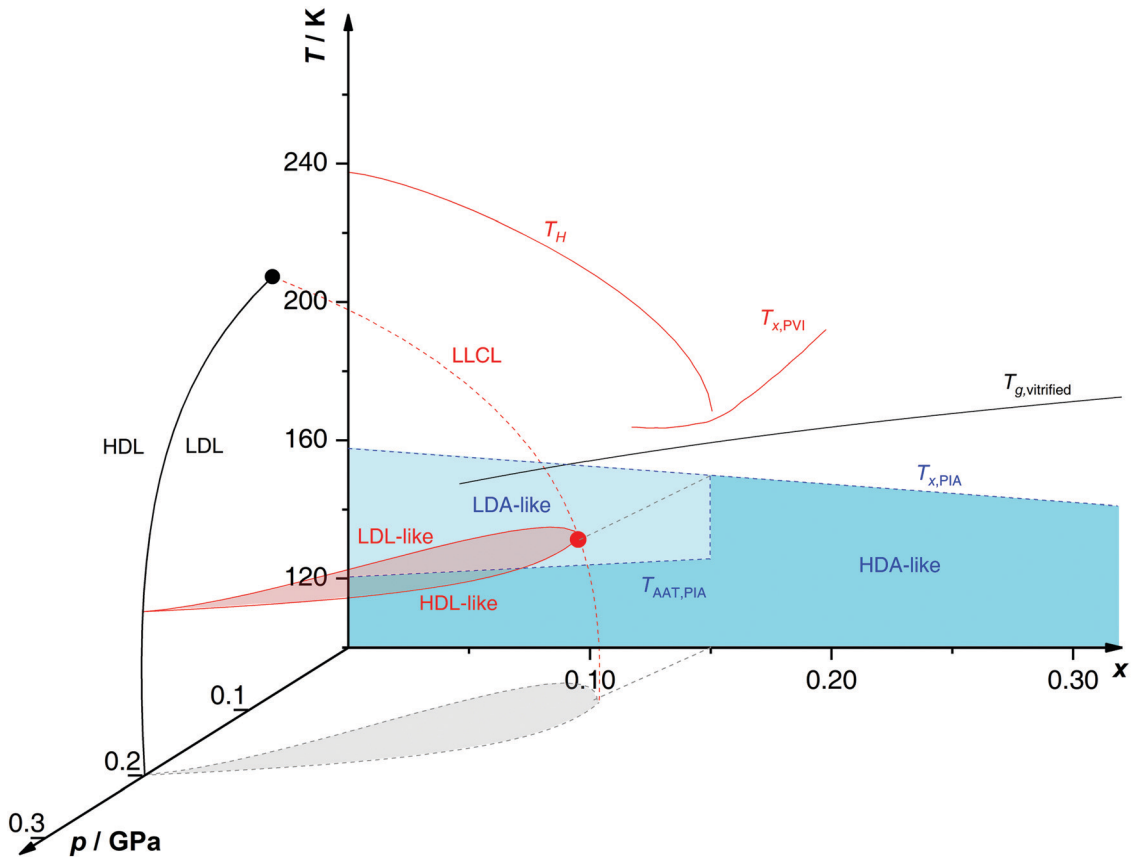

Fig. 10 Non-crystalline state diagram of glycerol–water. In black: the glass transition temperatures T_g of homogeneously vitrified solutions from ref. 218, and the LLCP of pure water (black circle) with the co-existence line between HDL and LDL from ref. 245. In red: polyamorphic behavior of emulsified PVI samples from ref. 230 and 244 with the homogeneous nucleation temperature T_H, the cold crystallization temperature T_x, the LLCL spawning from the pure water critical point, and the LLCP of x = 0.135 solution at 150 K and 0.045 GPa (red circle). In blue: polyamorphic behavior of PIA bulk samples heated at 1 bar according to ref. 224 with the polyamorphic transition T_{AAT}, the cold-crystallization temperature T_x and the end of polyamorphism at $x > 0.15$. The LLCP from ref. 230 is connected to the end of polyamorphism from ref. 224 *via* the grey line nearly parallel to the pressure axis, highlighting the liaison of both studies.

Indeed, it has been proposed that the LLCP of pure water in the p–T plane (x = 0) originates a line of LLCPs in the p–T–x space (red dashed line in Fig. 10). This liquid–liquid critical line (LLCL) moves towards lower T and p as x increases and extrapolates to T = 0 K at $x \approx 0.15$. It follows that, as $x \rightarrow 0.15$, the LLCP of the glycerol–water solution moves into the glass domain and hence, the LLPT vanishes. Consequently, the observation of the AAT requires the vitrification of dilute solutions, but cannot be observed in the intermediate, *i.e.*, glass-forming region (blue region in Fig. 9a). Procedures such as PVI, PIA or HYP are necessary to study polyamorphism in glycerol–water solutions.

Further support for the model of Biddle *et al.*[188] is provided by Raman data of Suzuki and Mishima[230] suggesting that glycerol is integrated homogeneously into water's H-bond network, both for the HDA and LDA matrix. Thus, the AAT may genuinely occur at constant x, *i.e.*, is isocompositional. This contrasts the behavior in salty solutions as, *e.g.*, described in Section 2.1.4 for the case of LiCl–H_2O, where pure water domains and concentration changes are involved in the AAT.

In addition, Suzuki and Mishima conducted more detailed Raman studies on the polyamorphic transition in glassy glycerol–H_2O solutions with x = 0.07 as a function of temperature.[246] When heating pressure-vitrified samples at ambient pressure the backbone of glycerol displays significant changes depending on whether the solvent water is in an HDA-like or LDA-like state. In particular this change in glycerol conformation is observed concomitantly with the polyamorphic transition, suggesting that water polyamorphism may also affect the structure and dynamics of solutes (*e.g.*, alcohols, polymers, proteins[247–252]).

3.1.3 Polyamorphism in samples produced by pressure-induced amorphization (PIA). Samples obtained by PIA of crystallized solutions yield results that are largely consistent with results obtained for PVI samples prepared by cooling at 0.3 GPa.[230] In aqueous glycerol solutions, PIA is in general possible as long as pure hexagonal ice precipitates from the solution. At 1 bar, this can be achieved by cooling glycerol–water solutions with $x \leq 0.32$ and using sufficiently slow cooling rates.[224] Unsurprisingly, PIA of crystalline solutions produces a high-density amorphous mixture where water is in an HDA-like state. As explained below, experiments suggest that glycerol is integrated into the HDA matrix during the compression process.[224] Among others this is derived from the increase of the onset pressure at which the crystallized solution becomes amorphous with increasing glycerol content.

When the HDA samples obtained by PIA are recovered and heated at 1 bar, the HDA → LDA transition takes place only at $x \leq 0.15$ although PIA still occurs in more concentrated solutions. At $0.15 < x \leq 0.32$ one broad cold-crystallization exotherm is observed around 140–160 K, followed by the glass transition of restored MFCS (see black curve in Fig. 8 for the x = 0.20 solution). That is, glass polymorphism at $0.15 < x < 0.32$ does not occur since LDA is suppressed at these concentrations. The absence of AAT/LLPT at $x > 0.15$–0.20 is reflected in Fig. 10 where above the critical concentration ($x \approx 0.15$) the LLCL cannot be crossed, no matter the chosen pressure and temperature.

The dominance of HDA/HDL-like components at such concentrations (emphasized in Fig. 9b) goes hand in hand with glass forming properties.[215] A preference for HDA/HDL states implies the suppression of crystallization because LDA/LDL is the precursor to ice I[151,157] (see Section 2.1.4). In Fig. 10 it is evident that the HDA → LDA polyamorphic transition at 1 bar shifts to slightly higher temperatures upon adding glycerol whereas LDA crystallization shifts to lower temperatures.[224] Consequently, the HDA state is stabilized over LDA with increasing x. The progress towards the high-density component is confirmed by very recent Raman experiments hinting that dissolved glycerol has a similar effect on the structure of water as pressure does.[244] This is similar to the case of aqueous electrolyte solutions,[153] *e.g.*, LiCl–H_2O (see Section 2.1.4), albeit without electro-restrictive forces but H-bonding as the source of the internal pressure.

In Fig. 11 we present novel data on the volume change associated with compression/decompression cycles in solutions with x = 0.04 (see Section 2.1.4 for similar experiments on LiCl–H_2O). The main goal is to test whether the LDA ↔ HDA (AAT) transformation found by Suzuki and Mishima[230] using homogeneous glassy samples prepared by PVI can also be observed in the heterogeneous samples prepared by PIA. The sudden density change at p = 0.06 GPa for the downstroke and at p = 0.45 GPa for the upstroke (red curve in Fig. 11) signifies the AAT in both directions. The similarity with the volume change of pure water under the same process (black curve in Fig. 11) indicates that the transformations observed in the mixture are due to water switching between LDA-like and HDA-like states.

This comparison shows (i) the densification for the LDA → HDA transition in glycerol–water solutions is smaller than in

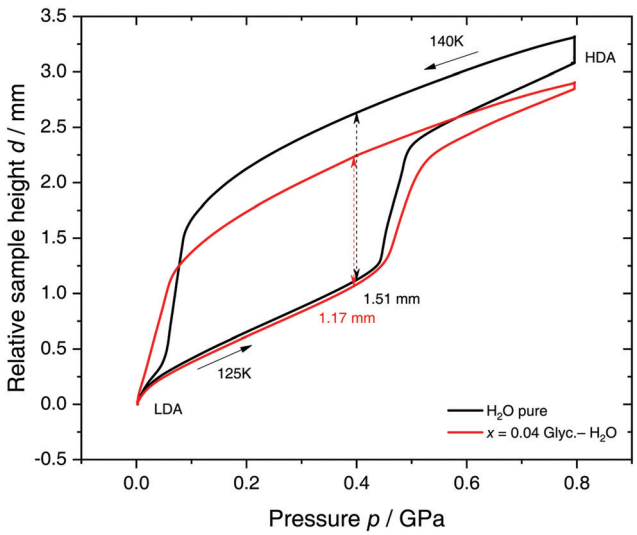

Fig. 11 Sample height changes upon decompression of HDA (140 K) and compression of LDA (125 K) for 300 μL x = 0.04 glycerol–water solution (red curve) and 300 μL pure water (black curve). The step height in glycerol–H_2O is reduced by ≈23% compared to pure water as indicated by the double-headed arrows. Cylindrical samples of 8 mm in diameter were prepared by PIA at 77 K followed by annealing at high pressures.

pure water and (ii) the LDA → HDA transformation is smoother when glycerol is present. Identical volumes of $x = 0.04$ glycerol–water solutions and pure water contain roughly the same number of water molecules. Thus, one would expect almost identical densification at the polyamorphic transition. However, the sample height changes are 1.51 mm and 1.17 mm for pure water and the glycerol–water mixture, respectively (double-arrows in Fig. 11), *i.e.*, the volume change during the LDA ↔ HDA transformation decreases roughly by 23% when glycerol is added ($x = 0.04$). This implies that not all water molecules experience the polyamorphic transition in the solution. The non-polyamorphic water molecules are in fact the ones that are trapped in the MFCS. These water molecules would account for ≈10% total step height decrease. However, Fig. 11 shows ≈23% difference in step height between black and red curves (see double headed arrows).

This can be explained by considering that (i) there are water molecules in the solution that do not exhibit polyamorphism (see Section 3.1.1), *e.g.*, water molecules located in the interphase (between MFCS and water domains), or (ii) by a smaller density difference between the LDA and HDA water domains within the glycerol–water than in the case of pure water. Our MD simulations show that adding glycerol considerably increases the density of the LDA solution while barely changing the density of the HDA solution,[253] supporting scenario (ii). Scenario (i) seems unlikely, since one would need more water molecules trapped in the interphase than in the MFCS. This would imply unreasonably large volumes of interphase in $x = 0.04$ glycerol–water. That is, we interpret these observations in the sense that the sample formed at high pressure by PIA consists of MFCS and HDA, which upon decompression converts to MFCS and LDA, where the LDA contains glycerol molecules, such that the LDA density significantly increases with increasing x. We note that our earlier experiments[224] and MD simulations,[253] as well as available experimental results[230,244,254] confirm that glycerol is soluble both in LDA and HDA. These observations are in striking contrast to LiCl–H_2O: whereas the difference in step height is slightly overestimated for LiCl–H_2O (see double headed arrows in Fig. 6), it is underestimated for glycerol–water.

Next, we discuss briefly the crystallization temperature T_x of glycerol–water solutions prepared by different methods. Depending on the procedure followed for sample preparation glassy glycerol–water solutions exhibit noticeable differences in T_x (which is not surprising since glasses in general are history-dependent materials). The crystallization temperatures of glycerol–water samples during isobaric heating are shown in Fig. 10 at 1 bar (T–x plane) for samples formed *via* PIA ($T_{x,\mathrm{PIA}}$, blue dashed line) and PVI ($T_{x,\mathrm{PVI}}$, red line). The spread between $T_{x,\mathrm{PIA}}$ and $T_{x,\mathrm{PVI}}$ is remarkable. In particular, we note that the PVI samples always crystallize at much higher temperatures than PIA samples (≈30 K difference at $x = 0.17$). Crystallization commences well above the T_g of a homogeneously vitrified solution at 1 bar[218] for the PVI samples but below T_g for the PIA samples. These differences in T_x can be due to three distinct causes: (i) PIA leads to heterogeneous amorphous samples consisting of water-rich and solute-rich domains, where crystallization of the water-rich domains takes place first, at temperatures similar to pure water; (ii) ice nucleation is triggered by the interphase[224] or remnants of the process of PIA;[255,256] or, (iii) an HDA-like sample does not experience the polyamorphic transition but instantly crystallizes to ice I. We regard (iii) to be unlikely since pure HDA samples are known to crystallize to high-pressure ice modifications (such as ice IV and ice XII).[257] (ii) was shown to occur for pure water as an increase of T_x by up to 11 K was observed after removal of nanocrystalline domains through annealing.[255,256] It is doubtful, however, whether the nanocrystalline/amorphous interphase in glycerol–water can also be removed with a similar procedure. (i) seems to be the most plausible explanation as complete homogenization after PIA is rather unlikely. This represents the main difference between samples prepared by PVI and PIA.

3.1.4 Polyamorphism in glycerol–H_2O solutions from computer simulations. The polyamorphic behavior of glassy aqueous solutions containing small molecules remains mostly unexplored in computational studies. In a recent work, we employed MD simulations to study the pressure-induced LDA → HDA transformations in glycerol–water mixtures.[253] Specifically, we studied the pressure-induced LDA → HDA transformation at various temperatures using the TIP4P/2005 water model and two glycerol models. The TIP4P/2005 water model exhibits a relatively sharp LDA → HDA transformation at low temperatures reproducing qualitatively the LDA → HDA transformation found in experiments.[91] This is an important feature of the TIP4P/2005 water model given that the compression/decompression rates accessible to MD simulations are much faster than the rates accessible to experiments; see Section 1 and ref. 119, 253 and 258 for a discussion of the rates used in MD simulations.

In order to study the LDA → HDA transformation in glycerol–water solutions, we first prepare glassy configurations at $T = 80$ K and $p = 0.1$ MPa, see Fig. 12a. These glassy mixtures are obtained by cooling an equilibrated (liquid) solution at constant pressure ($p = 0.1$ MPa) with a cooling rate $q_c = 1$ K ns^{-1}. At this cooling rate, crystallization is avoided and the aqueous solutions appear to be homogeneous. Instead, in the experiments of ref. 224, the cooling rates are slow, $q_c < 1$ K min^{-1}, and crystallization takes place at $x \leq 0.38$. The glassy solutions obtained using the HYP process in the MD simulations are comparable to the ones prepared by Suzuki and Mishima[230] using PVI, since in their experiments, the glasses are homogeneous and free of ice. The glasses prepared at $p = 0.1$ MPa and $T = 80$ K are then compressed at a compression rate of 100 MPa ns^{-1} (see Fig. 12b). During compression, at $T = 80$ K, the glassy solutions transform to the HDA state. However, the transformation becomes smoother with increasing glycerol content and the LDA → HDA transition in the mixtures is not observable for approximately $x > 0.05$. The underlying reasons for this are that (i) the density of the starting glassy mixture at $p = 0.1$ MPa increases rapidly during the preparation process (Fig. 12a), while (ii) the densities of the HDA solutions at $p > 1000$ MPa are practically independent of the glycerol

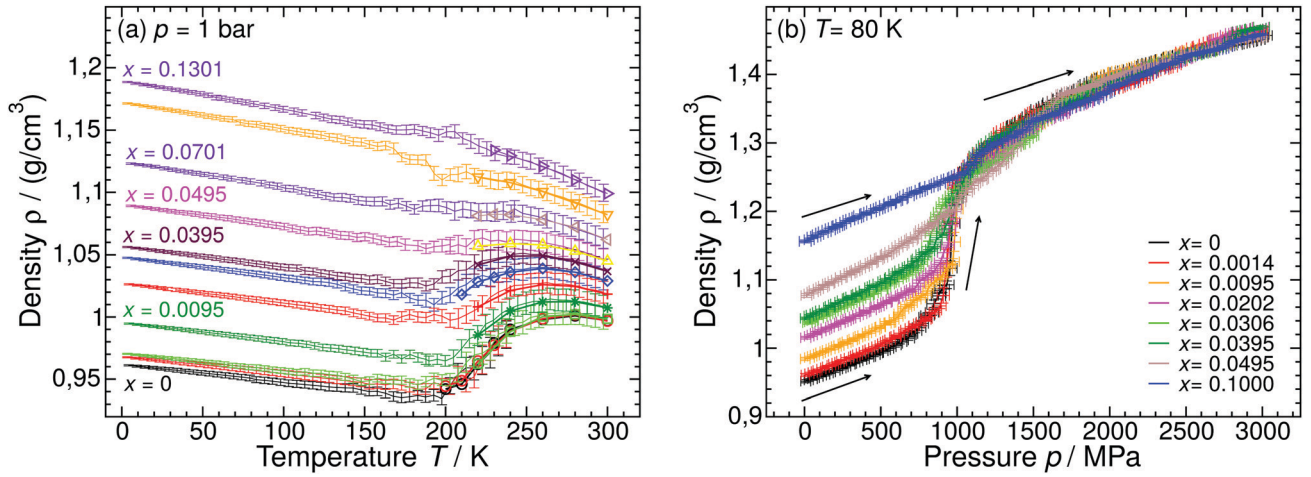

Fig. 12 (a) Density of glycerol–water solutions as function of temperature during cooling at p = 0.1 MPa from MD simulations (thin lines with error bars). The solutions are equilibrated at T = 300 K for $x > 0$ and T = 240 K for $x = 0$, and then cooled at rate q_c = 1 K ns^{-1}. Glycerol mole fractions are (bottom to top) x = 0 (black and red), 0.0014 (green), 0.0095 (dark green), 0.0202 (red), 0.0306 (blue), 0.0395 (maroon), 0.0495 (magenta), 0.0701 (violet), 0.10 (orange), and 0.1301 (indigo). For comparison, included are the densities of the solutions in equilibrium (symbols). The solutions are in the equilibrium liquid state at roughly $T > 200$ K and in the glassy state at approximately $T < 150$ K. Each data point during the cooling simulation is an average over a pressure window of 10 MPa and the error bars represent the standard deviation of the density over this p-interval. (b) Density as a function of pressure during isothermal compression at T = 80 K of the glassy solutions prepared in (a). At all temperatures, increasing glycerol concentration reduces the density change during the compression process. The LDA → HDA transformation can be identified at roughly $x \leq 0.05$. At higher concentrations, the density of the starting glass is high, $\rho \geq 1.1$ g cm^{-3}. The compression/decompression rate is q_p = 100 MPa ns^{-1}. Reproduced from ref. 253.

content ($x \leq 0.10$), see Fig. 12b. In other words, the starting glasses cannot reach an LDA state during cooling and they become more HDA-like with increasing x. The MD results are consistent with experiments that show that the LDA → HDA transformation in glycerol–water mixtures is undetectable for approximately $x > 0.10$–0.12.[230]

Regarding the decompression-induced HDA → LDA transitions, the simulations in ref. 253 show that this transformation is very smooth in glycerol–water mixtures, barely detectable at $T > 120$ K, and occurs at negative pressures. At comparable conditions, $T \approx 140$–155 K and $x < 0.10$–0.12, the experiments of ref. 230 indicate that the density change during the HDA → LDA transformation is relatively sharp and it occurs at positive pressures.[224,230,246,254] At the currently accessible compression/decompression rates in MD simulations, HDA does not seem to convert back to LDA at $T \leq 120$ K even if negative pressures are considered. Instead, the density of HDA decreases continuously until the glass finally fractures at $p \approx -800$ MPa. This is not inconsistent with the experiments of ref. 224 where it is shown that, upon decompression of the HDA-like mixtures, no transformation back to a less dense state occurs at T = 77 K and $p > 0$ MPa. We note that the MD simulations are able to reproduce the qualitative effects of varying T and x reported in experiments.[224,230] Specifically, increasing T leads to a reduction of the hysteresis in $\rho(p)$ during a compression–decompression cycle and increasing the glycerol content to smoother changes in $\rho(p)$ during the LDA → HDA transformation. Interestingly, the results from the MD simulations were robust, not sensitive to the glycerol model used, even when the specific conformations adopted by the different glycerol models in the glass state differ.[253,259]

One of the main contributions of MD simulations is to provide a molecular-level description of the LDA → HDA transformation in the glass states, information that is not easily accessible in experiments. The structural changes accompanying the LDA → HDA transformation in pure water are well-known (see, *e.g.*, ref. 260–262). Interestingly, similar structural changes are observed in the TIP4P/2005 glycerol–water mixtures. For example, Fig. 13 shows the water oxygen–water oxygen (Ow–Ow) radial distribution function in the LDA and HDA mixtures for $x \approx 0.03$. During the LDA → HDA transformation (black curves) the HB network collapses with roughly one molecule displacing from the second hydration shell of LDA ($r \approx 4.5$ Å) toward the first hydration shell ($r \approx 2.8$ Å), filling the first interstitial shell ($r \approx 3.5$ Å). One may wonder, if similar structural changes occur next to glycerol's OH groups. To show that this is indeed the case, we include in Fig. 13 (red lines) the RDFs of glycerol oxygens (Og) around water oxygens. Fig. 13 demonstrates that during the LDA → HDA transformation, glycerol Og atoms move closer to their nearest water neighbors, from the neighboring water molecule's second shell ($r \approx 4.5$ Å) toward their first shell and filling the corresponding first interstitial shell ($r \approx 3$–3.5 Å). However, and not surprisingly, the changes in the Ow–Og RDFs (red lines) are less pronounced than in the case of Ow–Ow RDFs (black lines) since a water molecule next to an OH group of glycerol is still surrounded mainly by other water molecules. We note that the role played by the glycerol model is relevant at the molecular level; specifically, the Og–Ow RDF is sensitive to the glycerol model considered.[253] Yet, for both models studied in ref. 253, Og atoms tend to populate the interstitial space of the neighboring water molecules ($r \approx 3$–3.5 Å) during the LDA → HDA transformation, as shown in Fig. 13.

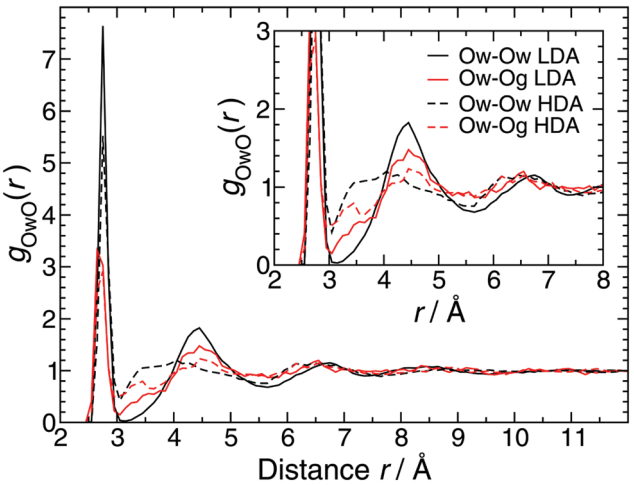

Fig. 13 Radial distribution function of water (Ow) and glycerol (Og) oxygen atoms around water oxygens Ow from MD simulations at T = 80 K and p = 0.1 MPa, and x = 0.0306. During the LDA → HDA transformation, the main change in both Ow–Og and Ow–Ow RDFs (red and black lines, respectively) is the decrease of the peak located at $r \approx 4.5$ Å (second hydration shell of water) and decrease in the depth of the minimum located at $r \approx 3.2$–3.5 Å (first interstitial shell of water). The inset shows a magnification of the most relevant region. Reproduced from ref. 253.

The similar collapse of the hydrogen bond (HB) network between water–water OH groups and water–glycerol OH groups is remarkable since it suggests that glycerol OH groups participate actively in the LDA → HDA transformation. In the case of non-hydrogen bonding solutes, such as ions, it is hard to imagine a shift of water molecules from a second hydration shell to a first interstitial shell, analogous to the HB collapse at water–water and water–glycerol OH groups. In this regard, the collapse of the HB network between water and alcohol OH groups makes alcohols rather special; alcohols allow for the suppression of ice (to a degree that depends on the type and the concentration of alcohol) while preserving the LDA → HDA transformation, at least in dilute solutions. It follows from the discussion above that molecules smaller than glycerol but with a high density of OH groups are good candidates to observe water glass polymorphism, provided they are also able to suppress crystallization. Candidates include, *e.g.*, hydrogen peroxide.

The effects of adding glycerol on polyamorphism of glycerol–water solutions can also be estimated by looking at the supercritical lines (ρ maxima, κ_T maxima and c_p maxima lines, see Fig. 1) in the supercooled solutions. For example, MD simulations of TIP4P/2005 water and the glycerol model based on ref. 263 show that the TMD line shifts towards lower temperatures with increasing glycerol concentrations.[259] This suggests that adding glycerol to water tends to shift the LLCP to lower temperatures. Such findings are also supported by experiments since the densities obtained from these MD simulations in the liquid state are in remarkable agreement with experimental data for approximately $x \leq 0.20$. Indeed, the computer simulations' results and experiments of glycerol–water solutions and brine–glycerol mixtures across the whole glycerol concentration range[264,265] indicate that the mixtures' densities for approximately $T < 350$ K are well described by the following expression $\rho(w_g, T) = (1 - w_g)\rho_w^0(T) + w\rho_g^0(T)$, where, $\rho_w^0(T)$ and $\rho_g^0(T)$ are the densities of pure water and glycerol at temperature T, respectively. Consistent with the observed shift in the TMD line, ref. 259 also shows that adding glycerol shifts the compressibility maximum and the c_p-maximum towards lower temperatures. In addition, we note that even for $x \leq 0.05$, the diffusivity of TIP4P/2005 water in the solutions does not show an FSDC, at least for $T \geq 210$ K (p = 0.1 MPa); at all concentrations the T-dependence of water diffusivity follows the Vogel–Fulcher–Tammann equation.[80,266]

3.2 Other alcohol–H_2O solutions

3.2.1 Experiments on LDA ↔ HDA in polyols–water. The glass transitions of vitrified aqueous alcohol/sugar solutions have been well-studied over many years, especially in the pharmaceutical sciences, *e.g.*, ref. 242 and 267–272 to only cite a few. Homogeneous vitrification, however, is only achieved in rather concentrated solutions where polyamorphism is suppressed. As of now the research on water's polyamorphism is limited to the work of Suzuki on the solutes ethylene glycol, glycerol (see above), *meso*-erythritol, xylitol and D-sorbitol.[244,254] Significantly extending his previous work,[230,246] Suzuki examined the polyamorphic transition in dilute emulsified aqueous solutions of these polyols (containing two to six hydroxy groups) in the range between x = 0.02–0.05 (0.08 for ethylene glycol).[254] That is, he performed decompression and recompression experiments between 130 K and 160 K on polyol solutions vitrified under pressure. In general the polyamorphic transition is observed in most of the solutions in this concentration range. However, near 150 K the samples tend to crystallize, as compared to 142 K for pure, bulk water (without emulsification), thereby hampering reversible cycling between HDA-like and LDA-like at even higher temperatures.[93,163] Only the rather concentrated solutions and/or solutes with more OH-groups (*e.g.* xylitol and D-sorbitol) still display the polyamorphic transition both on compression and decompression above 150 K. Generally, the transformation shifts to lower pressures with growing x. This effect is more pronounced for solutes with more OH groups. It is again possible to map co-existence regions of polyol solutions by inspecting the pressure hysteresis as was done in the glycerol–water study (see Fig. 10).[230] The corresponding LLCPs are estimated for ethylene glycol solutions at 145 K (due to intervening crystallization) and for the remaining other solutes at 150 K.[244]

The critical pressure of the LLPT does not depend on the type of solute but remains at 0.050 ± 0.005 GPa for all polyols. It is however evident that polyamorphism vanishes at lower concentrations for solutes with more OH-groups. This reflects more water molecules being directly bonded to a single polyol molecule, *i.e.*, less water molecules remain to form a H_2O-network. Consequently, near the critical concentration water forms mostly high-density states suppressing crystallization. Thus, it is not surprising that the homogeneous nucleation temperature T_H is lower for solutes with more OH groups.[254,273]

3.2.2 Computational studies on the LLCP in methanol–water. While there is solid evidence for the existence of LLCPs in polyol–water solutions from the experimental side,[230,244]

corresponding MD simulations of alcohols other than glycerol[253] are rather scarce. To our knowledge, the only computational study is the work of Corradini *et al.*[274] on the LLCP in methanol–water mixtures based on the TIP4P/2005 water model and the OPLS-AA model for methanol[275] at two mole fractions, $x = 0.05$ and 0.10.

The LLCP in TIP4P/2005 water has not been directly accessed at present as long simulation time scales are needed to equilibrate this water model. At present, the location of the LLCP in TIP4P/2005 water is estimated to be at 175–193 K (see Table 1). For example, a recent equation of state for TIP4P/2005 water has been obtained using a two-state water model.[54,58] This equation of state indicates that the LLCP should be located at T_c = 182 K, p_c = 170 MPa, and ρ_c = 1.017 g cm^{-3}. Similarly, an equation of state for TIP4P/2005 water based on the potential energy landscape approach predicts that T_c = 175 K, p_c = 175 MPa, and ρ_c = 0.997 g cm^{-3}.[55] In ref. 274, evidence of an LLCP at low temperatures was found for methanol–water solutions at $x = 0.05$ but not for $x = 0.10$. The LLCP location is estimated to be T_c = 193 K, p_c = 96 MPa, and ρ_c = 1.003 g cm^{-3}. This conclusion is based on (i) extrapolation of high-temperature isochores to low-temperatures, and (ii) the development of an inflection point in the isotherms upon cooling. The estimated LLCP location of the methanol–water solutions is almost identical to the location of the LLCP in bulk water in the early work of ref. 53. However, longer computer simulation times at low temperatures are needed in order to confirm the existence of an LLCP in methanol–water solutions of TIP4P/2005. We note that the MD simulation data of ref. 274, at the accessible equilibrium temperatures, are fully compatible with the predicted LLCP in methanol–water mixtures. Specifically, this study shows that the methanol–water solutions exhibit anomalous density maxima line in the p–T plane, as well as κ_T-maxima and α_p maxima lines at $T > T_c$. In particular, the κ_T and α_p maxima lines merge in the p–T plane upon cooling, as the hypothesized LLCP location is approached, in agreement with the scenario presented in Fig. 1.

The absence of an LLCP at $x = 0.10$ in ref. 274 is consistent with the location of the TMD lines in the p–T plane obtained for methanol–water solutions at different concentrations. Specifically, the TMD line of these solutions shifts towards lower temperatures as the methanol content increases, a result that is consistent with experiments.[276] The results from MD simulations suggest that the features of the phase diagram of water, including the LLCP, shift towards lower temperatures with increasing amounts of methanol.

4 Other solutes in water

4.1 Polar solutes

4.1.1 Proteins. Recently, the concept of water polyamorphism found its way into the field of biophysics as it was applied to cooled hydrated protein crystals. In general, the water properties are massively affected by the interaction with the protein. While not accessible in bulk water the FSDC at ambient pressure was inferred for protein hydration water.[247,249,250] Going beyond this dynamic transition, the work by Kim *et al.*[248,277–281] tackles structural transformations induced by pressure. When rapidly cooling a pressurized ($\approx$0.2 GPa) protein crystal, ice formation can be entirely avoided as indicated by X-ray studies.[279,280] Interestingly, the solvent water shows a similar diffraction pattern as HDA of neat water and features the transformations to LDA and ice I when heated at 1 bar. In the aftermath of the polyamorphic transition the protein crystal diffraction intensities decrease while simultaneously, mosaicity (*i.e.*, the spread of crystal plane orientations) increases, signifying crystal damage. This trend is more obvious in protein crystals with high solvent content, implying that the damage originates from transitions in solvent water[278] and not from X-ray radiation as it is the case at ambient temperature.[282,283]

For pressure-vitrified protein hydration water the diffraction profiles between 80 and 170 K can be expressed as a linear combination of a high-density state at 80 K and a low-density state at 170 K, suggesting an underlying first-order transition.[277] The authors also argue that the unusually small changes in unit cell volume can only be rationalized assuming liquidity of water molecules during the transition, where the high mobility makes them capable of leaving the protein crystal. An additional effect that was not considered by the authors might be that the density difference between the HDA- and LDA-state is diminished in the presence of solute compared to pure water, as is the case in glycerol–water solutions (see Section 3).[253] The dynamical transition between conformational states in pressure-vitrified proteins occurs already at very low temperatures (110 K) upon warming.[248] This finding is striking, as such transitions have previously been observed only around 180–240 K.[284,285] Interestingly, at 110 K also the polyamorphic transition of solvent water occurs.[248,281] However, when avoiding the formation of HDA-type hydration water by cooling an identical protein crystal at ambient pressure, no increase in protein mobility is visible up to 180–240 K. Thus, it seems that the HDA $\rightarrow$ LDA transition in pressure-vitrified hydration water is accountable for the protein dynamical transition at cryogenic temperatures, whereas the mobility in LDA-type hydration water is not sufficient to trigger the transition at 110 K. One could speculate that this results from the water molecules being more mobile in the HDA than in the LDA state. Indeed, it has been shown that the dynamics in HDA near 110 K are two orders of magnitude faster than in LDA,[286] reaching the relaxation times of an ultraviscous liquid. That is, the mobility of water is likely the driving factor for the conformational fluctuations of proteins as it has also been suggested in various MD simulation studies.[287–289]

The HDA $\rightarrow$ LDA transition kinetics also obeys the Avrami equation[236–238] implying an underlying mechanism of nucleation and growth, *i.e.*, a first order transition between two amorphous solids.[277] That low-density amorphous domains nucleate within the HDA-matrix, which then grow on the expense of it, was shown by Tonauer *et al.*[290] for the pure water case. This requires the development of sharp interfaces between two amorphous forms, a novel concept in glass physics observed first by Mishima *et al.*[291] and Winkel *et al.*[107]

4.1.2 Tartrates. The mobility of water molecules at the polyamorphic transition was further probed in pressure-vitrified sodium potassium tartrate solution[278] by manually cracking the frozen phase and monitoring its evolution.[281] The cracks persist as long as water is in the HDA state but crack healing is observed once the HDA → LDA transition is induced upon heating at ≈120 K and 1 bar. By contrast, samples vitrified at ambient pressure do not show crack healing until the LDA water crystallizes.[281] As crack healing requires rather high molecular mobility this strongly reinforces the argument that HDA turns into a mobile liquid at 120 K while LDA turns into a mobile liquid just before crystallization near 150 K.[90–93] This is consistent with calorimetric glass transition temperatures for HDA[83] and LDA.[100] Unexpectedly, the amorphous solutions do not crystallize to ice I but rather to host–guest compounds (type I clathrates) in which the tartrate is trapped in ice cages.[278] This suggests that tartrate can be, just like alcohols, dissolved both in the HDA and LDA matrix.

4.1.3 Hydrophilic-like monatomic solutes in a monatomic water-like model. Binary aqueous solutions were also studied by Le and Molinero[160] based on the coarse grained "model of water" (mW).[292] mW is a reparametrization of the Stillinger–Weber potential,[293] and represents water molecules as "atoms" with anisotropic interactions. mW "molecules" interact *via* a Lennard-Jones pair potential plus a three-body interaction term that favors local tetrahedral arrangements of an mW molecule and its four nearest-neighbors. mW calculations are fast compared to calculations using full-atomistic water models, including the TIP4P and SPC/E models, because they are based on short range interactions and do not include explicit partial charges (long-range interactions). Accordingly, mW is useful to study slow processes in water, such as ice nucleation. However, the absence of explicit charges can be problematic to model ions. In the context of this perspective, mW is interesting because it (i) clearly shows the existence of LDL-like and HDL-like states at high temperature and (ii) does not exhibit an LLPT/LLCP,[294,295] since crystallization, which is hardly avoidable at low temperature, prevents access to a possible LLPT. This provides a different scenario from the LLPT scenario of Fig. 1. The smallest cooling rate that can be used to vitrify liquid mW upon cooling at normal pressure is q_c = 10 K ns^{-1} [296] while the smallest experimental rate that avoids crystallization is $q_c \approx$ 0.001–0.01 K ns^{-1}.[89,112] In the glass state, the LDA → HDA transformation is very smooth, relative to full-atomistic polyamorphic water models, such as the ST2 model. Ref. 297 presents a scenario for glassy states of mW in which there is only a single liquid and two amorphous states that meet at a triple point rather than the LLCP scenario in other (full-atomistic) water models.

Le and Molinero[160] studied a binary mixture consisting of mW and a generic hydrophilic solute S with mole fractions x = 0–0.50. During out-of-equilibrium MD simulations the liquid was vitrified at ambient pressure and q_c = 10 K ns^{-1}. Depending on the solute concentration, three scenarios are distinguished: (i) at x = 0.50, the solutions crystallize into a homogeneous mW–S crystal of intercalated planes of S and mW molecules, (ii) at x = 0.20–0.40, a homogeneous glass is obtained, and (iii) at x = 0.05–0.15, a nano-segregated glass is formed. These nano-segregated glasses consist of two domains with a characteristic dimension of ≈5 nm. One domain resembles LDA, the other consists of a concentrated glassy solution of S and mW. The results of ref. 160 suggest that LDL is a poor solvent for the hydrophilic solute S due to the tetrahedral order of LDL. This forces the solution to phase-separate during the (fast) cooling process (x = 0.05–0.15), leading to the formation of LDA and glassy solution domains. Interestingly, Le and Molinero further point out that the S–mW water solutions exhibit some similarity with real LiCl–, NaCl–, and KCl–water solutions.[131] Specifically, in both cases there is phase separation into LDA and a salty glass even for hyperquenched samples, and the fraction of LDA in the glassy mixtures decreases linearly with x.

Although the S–mW water solution is not truly a salt–water mixture, these MD simulations present a picture of how phase separation may occur in real aqueous solutions. In particular, they show the important role that the presence of polyamorphism may have in salty solutions at low temperatures. We note that the effects of S–S and S–mW interactions should be taken into consideration when interpreting these results. Specifically, the generic hydrophilic solute S was not parameterized to reproduce any salt and the S–S interactions are very weak compared to S–mW interactions, which is not expected to be the case for, *e.g.*, Li^+ and Cl^- ions in aqueous solution.

4.2 Apolar solutes

Experimental studies on polyamorphism in the presence of apolar solutes are scarce, or in fact non-existent. At least we are not aware of any publication detailing the influence of apolar solutes on the polyamorphic transition of water. This would certainly be a topic worthwhile of study. However, both MD simulations and thermodynamic approaches have been pursued.

4.2.1 Hydrophobic-like solutes in a monatomic water-like liquid. Computer simulations of atomistic core-softened pair potentials have been used extensively in the past to elucidate the qualitative behavior of the thermodynamic and dynamical properties of water (see, *e.g.*, ref. 74, 298 and 299). These pair potentials involve a hard-core and a repulsive soft-core represented by a shoulder (see Fig. 14a). When parameterized properly, core-softened pair potentials can reproduce many of the anomalous features of water. One of the most successful water-like pair potentials is the Jagla model[299–301] (see Fig. 14a). As shown schematically in Fig. 14b, the Jagla potential exhibits a TMD line as well as the lines of maxima in c_p, κ_T, and diffusivity,[302–305] consistent with MD simulations of full-atomistic water models. In addition, it shows an LLPT and an LLCP at low temperatures (Fig. 14b) and glass polymorphism between LDA and HDA.[78,300,301,305,306] Jagla-like pair potentials can also exhibit pressure-induced amorphization of low-density crystals and two glass transition temperatures,[307–309] consistent with experiments[83,105,106] and computer simulations of full-atomistic water models.[115,159,166,167,258] However, contrary to the case of full-atomistic water models, reported Jagla-like

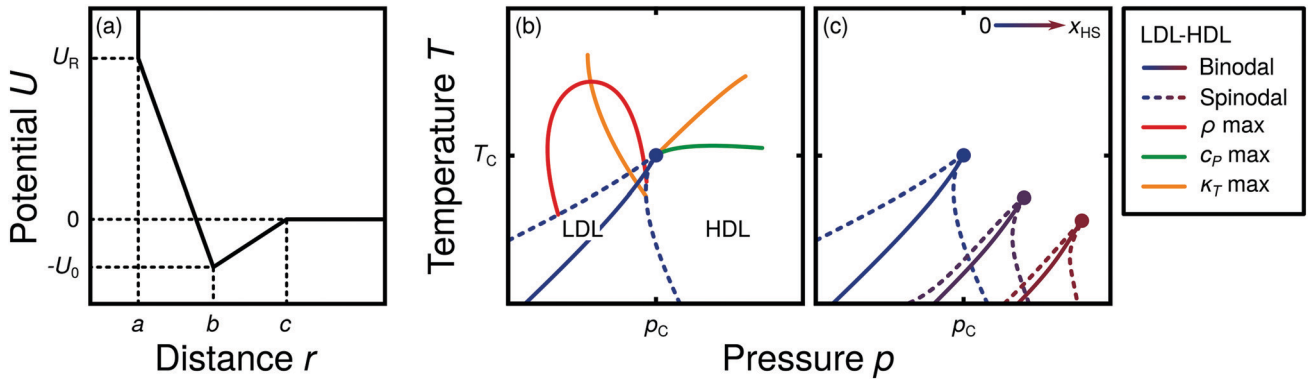

Fig. 14 (a) The Jagla pair potential consists of two length scales defined by the hard-core distance, *a*, and the location of the potential minimum, *b*. The core-softened part extends between *a* and *b*. (b) State diagram of Jagla potential based on ref. 78 and 305. The blue features show the LLCP with associated binodal and spinodal lines. The extrema in density (red) and thermodynamic response functions, heat capacity (green) and compressibility (orange), are also shown. Note that the LLCP binodal line has a positive slope, in contrast to the negative slope for water models (see Fig. 1). (c) Effect of increasing concentration on the LLPT of solution composed of Jagla water-like particles and hard spheres (from ref. 312). Contraction increases from blue to maroon color, blue lines are taken from (b).

potentials exhibit an LLPT line with positive, null, or mildy negative slope in the p–T plane (Fig. 14b), while full-atomistic models only show a negatively sloped LLCP line. Jagla-like models can also exhibit two κ_T maxima lines in the proximity of the LLCP, instead of one.

Relevant to this work is that aqueous solutions of small hard spheres in a Jagla-particle solvent describe many properties of binary aqueous solutions containing small hydrophobic solutes. Specifically, they can show a minimum in the solubility of small hard spheres as function of temperature.[310] This is consistent with experiments of small apolar solutes, such as alkanes and noble gases, in water where a solubility minimum occurs at $T \approx 310$–350 K.[310,311]

MD simulation studies of hard-sphere solutes in a Jagla solvent are reported in ref. 312 and 313. The model mixture employed in these works is identical to the model system studied in ref. 310. At the mole fractions, $x = 0.10$–0.50 with a total of 1728 particles, the solutions do not phase-separate and hence, the low temperature domain of the mixtures can be investigated. In ref. 312, discrete MD simulations are used to characterize the effects of concentration on the location of the LLPT/LLCP. This study shows that (i) an increase in solute concentration shifts the LLCP to lower T and higher p (see Fig. 14c). In addition, (ii) all solutions studied exhibit an FSDC upon isobaric cooling at $T > T_c$, in the proximity of the LLCP. In particular, the Widom line shifts towards higher p and lower T upon increasing x, consistent with the shift in the location of the LLCP.[313] (iii) In the case of $x \leq 0.40$, a TMD line is found which, again, shifts towards higher p and lower T upon increasing x. Interestingly, (iv) the shift of the LLPT towards higher p leads to a stabilization of the LDL phase with increasing concentration and a reduction of the co-existence region (Fig. 14c). The increased stability of LDL in the presence of apolar solutes contrasts the increased stability of HDL in ionic solutions.[47,144–148]

Points (i)–(iv) could be due to the fact that in the Jagla model liquid, the LDL is a better solvent for the hard spheres considered.[312] Interestingly, the MD simulations of ref. 48, based on TIP5P-Ew water and argon-like particles, also show that the solubility of the argon-like solute in TIP5P-Ew water is higher in LDL than in HDL.

We note that, when extrapolating the results of aqueous solutions based on the Jagla model to real aqueous solutions, one must take into consideration that the slope of the LLPT is positive, $\mathrm{d}p/\mathrm{d}T|_{\mathrm{LLPT}} > 0$, while $\mathrm{d}p/\mathrm{d}T|_{\mathrm{LLPT}} < 0$ in full-atomistic water models that show polyamorphism. The value of $\mathrm{d}p/\mathrm{d}T|_{\mathrm{LLPT}}$ specifies the entropy difference between LDL and HDL. Indeed, the Clapeyron equation indicates that $\mathrm{d}p/\mathrm{d}T|_{\mathrm{LLPT}} = \Delta S/\Delta V$, where ΔS and ΔV are the changes in entropy and volume across the LDL → HDL first-order phase transition. It follows from this relationship that, in the Jagla solvent, the LDL has a larger entropy than HDL while in water, HDL is the liquid with the higher entropy. A change in the slope of the LLPT can affect the thermodynamic picture of the model considered.[314] For example, as shown in ref. 303, 305 and 307, as the LLPT line in the p–T plane becomes parallel to the T-axis, the c_p-maxima line at $T > T_c$ vanishes.

4.2.2 Thermodynamic models. The behavior of the LLCP upon the addition of hydrophobic solutes was also studied on theoretical grounds.[188,315,316] In ref. 315 and 316 the canonical partition function for a family of binary solutions is considered and the corresponding phase behaviors are explored using numerical calculations. The theoretical models for the solutions are based on the van der Waals model and complemented by terms to account for the presence of hydrogen bonds. The key parameters of these models are a, the strength of the van der Waals attraction, and b, the excluded volume. Chatterjee and Debenedetti[316] studied three solutes with differing strength of the van der Waals attraction a and found that two of the three solutes shift the LLCP to higher T and lower p as concentration increases. This leads to a critical line emanating from the LLCP which is related to a similar line associated with the liquid–gas critical point. The manifestation of this relation is a closed loop immiscibility region in the T–ρ plane. For the third set of parameters the critical line emanating from the LLCP merges

with yet another of the five critical lines identified in the binary solution.[316] Cerdeiriña and Debenedetti[315] vary both a and b and find that the ratio a/b determines the magnitude and the direction of the LLCP shift as x is increased. Sufficiently large solutes shift the LLCP to higher T and lower p with increasing solute concentration. However, when the interaction a between water and solvent is strong the shifts are much smaller. The authors suggest that such a behavior might be found in solutions containing moderately large amphiphilic molecules.[315]

5 Conclusions and outlook

The intriguing concepts of polyamorphism, dating back to experiments in 1984,[109] and liquid–liquid phase transition (LLPT), dating back to simulations in 1992[33] are possibly related to the anomalous nature of liquid water. Although aqueous solutions have been a traditional topic in physics and chemistry for centuries, the study of polyamorphism in aqueous solutions has only emerged in the third millennium. Here, both computer simulations and experiments have advanced the frontiers of the field, where simulations mostly cover supercooled solutions and experiments mainly cover the amorphous solid. There are notable exceptions in which solid state polyamorphism is tackled in simulations[253] and in which the LLPT is addressed in experiments.[107,152,230]

Aspects such as phase separation, including ice formation, are common for experimentalists, limiting the accessible T and p region where solutions can be studied in the supercooled and glassy states. Crystallization is usually not an issue in computer simulations because of the small time scales currently accessible in MD simulations. In some sense, computer simulations and experiments complement each other by exploring different time scales. Computer simulations have explored time scales of $\leq$10 μs while experiments usually employ time scales of the order of minutes. However, the different time scales also imply that a direct comparison between simulations and experiments must be done carefully. Interestingly, for the case of pure water, the LDA → HDA transformation pressure at T = 80 K obtained in MD simulations at different compression rates extrapolates remarkably well to the experimental value.[119] We note that the ever increasing computational power makes it possible to probe equilibrium systems at lower and lower temperature, and allows the application of smaller and smaller rates, thereby reducing the gap to experiments. As of now only one simulation study has reached the cooling rates used in hyperquenching experiments, while compression rates are still at least three orders of magnitude larger than the highest rate accessible to experiments.[119] At the same time experimental techniques and procedures are constantly refined, making very high rates available and producing samples that could be in equilibrium at constantly lower temperatures, reducing the gap to simulations. Both approaches can also join the effort to study new systems, *i.e.*, solutions, where the problems of equilibration and crystallization do not interfere, opening the possibility for direct evidence of a liquid–liquid critical point (LLCP).

The solutes discussed in this perspective encompass ionic, polar and hydrophobic substances where the latter have barely received any attention. Although NaCl could be considered the archetype of an ionic solute, all experiments on polyamorphism focus on LiCl–water. LiCl solutions on the other hand have only been investigated in a single study employing computer simulations,[136] with almost all numerical studies on the LLPT devoted to NaCl–water. This testifies the separation between the two groups. As a model substance for polar solutes both communities study almost exclusively alcohols, where the benchmark case is glycerol. As of yet, literature on aldehydes, ketones, carboxylic acids *etc.* awaits publication.

In the present work we consolidate the computational and experimental work related to glass polymorphism and the LLPT of the last two decades. These studies are put into the context of the pioneering studies on vitrification of binary aqueous solutions. We augment this literature review with some original experiments aimed at resolving open questions. In this concluding section we attempt to elaborate on the difference between the solutes, especially alkali chlorides and glycerol. All solutions have in common that there is a concentration regime in which polyamorphism and LLPT are absent. This is always the case above the eutectic concentration (mole fraction $x \geq 0.28$ for glycerol, $x \geq 0.12$ for LiCl) but also even below (*e.g.*, $x \approx 0.15$ in glycerol–H_2O).[224,230] In dilute solutions ($x < 0.05$) the situation fundamentally changes and water may either occupy high-density or low-density states with a sharp first-order like transition between the two. These are the hallmarks of polyamorphism at low temperatures and the LLPT at high temperatures. A challenge in experiments is that dilute aqueous solutions, just like pure water, are bad glass-formers. That is, at standard cooling rates they crystallize (fully or partly), rather than vitrify. Hence, elaborate experimental techniques are required to study dilute amorphous solutions, such as hyperquenching (HYP), pressure-vitrification (PVI) and pressure-induced amorphization (PIA) of ice crystals. This has long been a disincentive for researchers to enter the field of polyamorphism in aqueous solution. Even if crystallization is avoided phase separation may interfere in salt solutions where water-rich and solute-rich liquids demix upon cooling.[126] This demixing takes place not only for slowly cooled salt solutions but also for HYP[131] and possibly PVI samples.[132,133]

By contrast, such behavior has not been reported in alcohol–water solutions. Instead, isocompositional vitrification takes place, both at ambient and high pressure. The variable pressure determines whether the dilute liquid solution turns into low-density amorphous (LDA) or high-density amorphous (HDA) ice upon cooling. Interestingly, increasing solute concentration and pressurizing seem to have similar effects on water's structure,[153,244,253] forcing the solvent water into the HDA state. HDA-like patches form even around tiny amounts of salt whereas tiny amounts of alcohol are not sufficient to enforce HDA structures. In fact, alcohols can also be surrounded by LDA type solvent depending on the pressure used for vitrification. Simulations show a continuous development of the LDA type solvent towards higher densities with increasing x.[253]

In other words, only salts but not alcohols are insoluble in LDA. Nonetheless, the phase segregation to concentrated salty solution and LDA might be prevented on kinetic grounds for rapidly cooled solutions, as testified by a strong variation of T_g of hyperquenched solutions with x. Consequently, the polyamorphic transition between LDA and HDA in alcohol solutions appears to be of isocompositional nature. On the other hand, this might not be so in salt solutions where the LDA ↔ HDA transformation seems to take place in the salt free parts of the sample. That is, polyamorphism in salt solutions is only preserved due to phase separation.

The influence of solutes on the LLCP locus has been addressed in simulations and thermodynamic models. Currently, the best estimate for the LLCP of pure water in experiments is 0.05 GPa and 223 K.[71] In general, the addition of solutes shifts the LLCP where direction and size of the shift depend on the type and concentration of the solute. While increasing x of NaCl moves the LLCP to lower (even negative) pressures and higher temperatures,[144] hydrophobic solutes show the opposite effects.[312]

Despite the fact that the general picture presented here is largely coherent, there are still several details that need further investigation. A non-exhaustive list of these open questions comprises:

(i) Is it valid to connect the LLCP of water as a single component to the line of LLCPs in a binary (alcohol) solution?
Suzuki and Mishima[230,244] locate the LLCPs in solutions by looking for the maximal concentration $x(T)$ at which the polyamorphic transition can be observed and link these points with the LLCP in pure water. It is however unclear whether the end of polyamorphism in binary solutions is associated with the kind of critical phenomena known for critical points in a single component, such as opalescence or divergences in thermodynamic response functions.

(ii) Are all salts immiscible with LDA?
While the work by Hofer *et al.*[130,195] and Ruiz *et al.*[129] suggests the possibility of small amounts of salts retained in LDA, Suzuki and Mishima,[134] Le and Molinero[160] and Corti *et al.*[156] support immiscibility.

(iii) Do LiCl–solutions phase-separate upon cooling under pressure?
Kanno[132] and the early work of Suzuki and Mishima[133] suggest phase segregation into concentrated solution and rather pure HDA whereas Suzuki and Mishima[134,152] assume homogeneous vitrification in their later publications.

(iv) What is the origin of the drift anomaly present in DSC scans of crystallized glycerol–water solutions?
Inaba and Andersson[221] explain it through cold-crystallization of dilute solution and melting of ice in concentrated solution taking place simultaneously while Feldman *et al.*[217,225] propose an interfacial liquid layer, exchanging water molecules with its surroundings. We suggest that it can be explained by the melting of an interphase sandwiched between bulk ice and maximally freeze-concentrated domains.[224]

(v) How different are the high-density solutions prepared by PVI and by PIA of solutions containing ice?
Both routes seem to lead to an indistinguishable HDA state for pure water.[113] For salt solutions the process of PIA undoubtedly starts from a phase segregated mixture whereas for PVI a homogeneous glass is inferred. Thus, the question is whether homogenization takes place upon PIA. This question has not been addressed directly so far since PVI was studied in Japan[152,230] and PIA in Austria[129,224] by different groups. Some indirect evidence suggests that PIA samples are heterogeneous, composed of (M)FCS and HDA, whereas PVI samples might either be homogeneous or heterogeneous (see (iv)).

(vi) Is it possible to design solutes with desired properties, *e.g.*, increased resistance against crystallization in solution such that the ''no man's land'' can be entered?
Promising evidence for this case has been provided by ionic liquids that mix ideally with water.[203] However, further work is needed for a conclusive answer. Extension of the work of ref. 203 and 206 to other ionic liquids would be very helpful. In particular, additional structural studies and compression/decompression experiments are desirable.

(vii) How do the kinetics of cold-crystallization differ from the kinetics of an LLPT?
This question has been touched in the work of Bruijn *et al.*,[233] but has remained at an inconclusive stage. In the future, we expect strong effort to resolve the remarkably complex mechanism of nucleation and growth,[317] which led to the controversy associated with the LLPT in glycerol–water solutions. Another important goal is to determine the rates of (cold-)crystallization and compare them with the kinetics of the LLPT at various temperatures and glycerol concentrations. Due to increasing viscosity upon adding glycerol crystallization rates are expected to slow down,[229] thereby facilitating access to the LLPT. Such kinetics studies might also help finding the missing link between the rates of crystallization of liquid and of cold-crystallization of amorphous solid.[318]

(viii) Can the gap between experiments and simulations be closed?
This encompasses not only the considerable disparities between cooling/compression rates in experiments and simulations but also the type of solutions studied. Obviously, detailed MD simulation studies on LiCl–water would greatly improve our understanding of the LLPT/LLCP in these solutions. Similarly, more experimental work on the polyamorphism in NaCl–solutions is desired to complement the results from simulations.

(ix) What kind of water–solute interactions may contribute actively in the LDA–HDA transformation of water?
For example, in the case of glycerol, the OH groups of the solute seem to help the LDA → HDA transformation to evolve during compression, since a collapse of the HB network next to glycerol's OH groups occurs, just as it is

found in bulk water. Instead, this is not the case for salts.

(x) Does the hydration water trigger dynamics in the solutes?

The studies on polyamorphism in pressure-vitrified protein solutions show a dynamical transition at surprisingly low temperature, when compared to the dynamical transition in ambient pressure cooled protein solutions. This low temperature transition has thus been associated with polyamorphism and the much higher mobility of water when in the HDA state. Very recently, a regular dynamical transition was observed for the first time in a non-biological macromolecule.[319] This offers the possibility to study a wider array of pressure-vitrified macromolecule solutions. If a low temperature dynamical transition would be observed independently of the chemical nature of the macromolecule this transition is highly likely related to the unique behavior of water alone.

(xi) How do hydrophobic solutes influence polyamorphism in H_2O?

So far hydrophobic solutes have only been studied in simple theoretical models. Hence, it would be promising to conduct experiments and full-atomistic simulations on polyamorphism in the presence of hydrophobic solutes. This is desirable since simulations in the Jagla model indicate a higher solubility of apolar solutes in LDA than HDA, which is the exact opposite from the observation in experiments on polar and ionic solutes.

We regard these eleven questions to be the most relevant questions in the field, which is still in its infancy given that it is less than two decades old, with only a handful of groups actively pursuing research in this direction. We hope that the present work highlighting the discrepancies and similarities between different systems and techniques as well as relevant open questions, will provide impetus to the field of liquid and glass polymorphism in aqueous solutions. Our ultimate goal is to inspire and motivate more researchers from experiment, simulation and theory to venture into the field and attempt "to boldly go where no man has gone before".[320]

Glossary of abbreviations

AAT	Amorphous–amorphous transition
BDS	Broadband dielectric spectroscopy
CS	Concentrated solution
DSC	Differential scanning calorimetry
DTA	Differential thermal analysis
FCS	Freeze-concentrated solution
FSDC	Fragile to strong dynamical crossover
HB	Hydrogen bond
HDA	High-density amorphous ice
HDL	High-density liquid
HYP	Hyperquenching
IMM	Immiscibility
IR	Infrared
LDA	Low-density amorphous ice
LDL	Low-density liquid
LLCL	Liquid–liquid critical line
LLCP	Liquid–liquid critical point
LLPT	Liquid–liquid phase transition
MC	Monte Carlo
MD	Molecular dynamics
MFCS	Maximally freeze-concentrated solution
PIA	Pressure-induced amorphization
PVI	Pressure-vitrification
QM/MM	Quantum mechanical/molecular mechanical
RDF	Radial distribution function
S	Solute
TMD	Temperature of maximum density
VHDA	Very high-density amorphous ice

Conflicts of interest

There are no conflicts to declare.

Acknowledgements

We are indebted to all the colleagues whose work on aqueous solutions has inspired us over the years, including (in alphabetical order) C. Austen Angell, Roland Böhmer, Livia E. Bove, Sergey V. Buldyrev, Frédéric Caupin, Pablo G. Debenedetti, Paola Gallo, Chae Un Kim, Osamu Mishima, Maria-Antonietta Ricci, Francesco Sciortino, H. Eugene Stanley, Yoshiharu Suzuki, and Edward Whalley. Financial support by the Austrian Science Fund (FWF project I1392 to TL and Erwin Schrödinger Fellowship J3811 N34 to PHH) and the University of Innsbruck (NWF-Project 282396 to PHH) is gratefully acknowledged.

References

1 S. T. Coleridge, The Rime of the Ancyent Marinere, in *Lyrical Ballads*, ed. W. Wordsworth and S. T. Coleridge, Routledge, 2nd edn, reprint edn, 1996.
2 Iron Maiden, Rime Of The Ancient Mariner, Powerslave, 1984.
3 F. Hofmeister, *Arch. Exp. Pathol. Pharmakol.*, 1888, **25**, 1–30.
4 F. Franks, *Water, a comprehensive treatise*, Plenum, New York, 1972.
5 R. O. Watts, E. Clementi and J. Fromm, *J. Chem. Phys.*, 1974, **61**, 2550–2555.
6 E. Clementi and H. Popkie, *J. Chem. Phys.*, 1972, **57**, 1077–1094.
7 H. Kistenmacher, H. Popkie and E. Clementi, *J. Chem. Phys.*, 1973, **58**, 5627–5638.
8 H. Kistenmacher, G. C. Lie, H. Popkie and E. Clementi, *J. Chem. Phys.*, 1974, **61**, 546–561.
9 R. Car and M. Parrinello, *Phys. Rev. Lett.*, 1985, **55**, 2471.
10 L. M. Ramaniah, M. Bernasconi and M. Parrinello, *J. Chem. Phys.*, 1999, **111**, 1587–1591.
11 B. M. Rode, C. F. Schwenk, T. S. Hofer and B. R. Randolf, *Coord. Chem. Rev.*, 2005, **249**, 2993–3006.

12 T. S. Hofer, A. K. H. Weiss, B. R. Randolf and B. M. Rode, *Chem. Phys. Lett.*, 2011, **512**, 139–145.
13 P. T. Kiss and A. Baranyai, *J. Chem. Phys.*, 2013, **138**, 204507.
14 P. T. Kiss and A. Baranyai, *J. Chem. Phys.*, 2014, **141**, 114501.
15 H. Jiang, Z. Mester, O. A. Moultos, I. G. Economou and A. Z. Panagiotopoulos, *J. Chem. Theory Comput.*, 2015, **11**, 3802–3810.
16 P. Ball and J. E. Hallsworth, *Phys. Chem. Chem. Phys.*, 2015, **17**, 8297–8305.
17 Y. Marcus, *Chem. Rev.*, 2009, **109**, 1346–1370.
18 K. A. Dill, T. M. Truskett, V. Vlachy and B. Hribar-Lee, *Annu. Rev. Biophys. Biomol. Struct.*, 2005, **34**, 173–199.
19 Y. Marcus and G. Hefter, *Chem. Rev.*, 2006, **106**, 4585–4621.
20 P. Jungwirth, B. J. Finlayson-Pitts and D. J. Tobias, *Chem. Rev.*, 2006, 1137–1139.
21 P. Jungwirth and B. Winter, *Annu. Rev. Phys. Chem.*, 2008, **59**, 343–366.
22 T. Encrenaz, *Annu. Rev. Astron. Astrophys.*, 2008, **46**, 57–87.
23 K. I. Öberg, *Chem. Rev.*, 2016, **116**, 9631–9663.
24 C. A. Angell, *Chem. Rev.*, 2002, **102**, 2627–2650.
25 M. Chaplin, Water structure and science, http://www1.lsbu.ac.uk/water/.
26 P. G. Debenedetti, *J. Phys.: Condens. Matter*, 2003, **15**, R1669–R1726.
27 I. Brovchenko and A. Oleinikova, *ChemPhysChem*, 2008, **9**, 2660–2675.
28 P. H. Handle, T. Loerting and F. Sciortino, *Proc. Natl. Acad. Sci. U. S. A.*, 2017, **114**, 13336–13344.
29 P. H. Poole, I. Saika-Voivod and F. Sciortino, *J. Phys.: Condens. Matter*, 2005, **17**, L431.
30 R. J. Speedy, *J. Phys. Chem.*, 1982, **86**, 982–991.
31 S. Sastry, P. G. Debenedetti, F. Sciortino and H. E. Stanley, *Phys. Rev. E: Stat. Phys., Plasmas, Fluids, Relat. Interdiscip. Top.*, 1996, **53**, 6144–6154.
32 L. P. N. Rebelo, P. G. Debenedetti and S. Sastry, *J. Chem. Phys.*, 1998, **109**, 626–633.
33 P. H. Poole, F. Sciortino, U. Essmann and H. E. Stanley, *Nature*, 1992, **360**, 324–328.
34 O. Mishima and H. E. Stanley, *Nature*, 1998, **396**, 329.
35 C. A. Angell, *Science*, 2008, **319**, 582–587.
36 P. Gallo, K. Amann-Winkel, C. A. Angell, M. A. Anisimov, F. Caupin, C. Chakravarty, E. Lascaris, T. Loerting, A. Z. Panagiotopoulos, J. Russo, J. A. Sellberg, H. E. Stanley, H. Tanaka, C. Vega, L. Xu and L. G. Pettersson, *Chem. Rev.*, 2016, **116**, 7463–7500.
37 A. Nilsson and L. G. Pettersson, *Nat. Commun.*, 2015, **6**, 8998.
38 M. A. Anisimov, M. Duska, F. Caupin, L. E. Amrhein, A. Rosenbaum and R. J. Sadus, *Phys. Rev. X*, 2018, **8**, 011004.
39 D. Paschek and R. Ludwig, *Angew. Chem., Int. Ed.*, 2014, **53**, 11699–11701.
40 F. H. Stillinger and A. Rahman, *J. Chem. Phys.*, 1974, **60**, 1545–1557.
41 F. Smallenburg, P. H. Poole and F. Sciortino, *Mol. Phys.*, 2015, **113**, 2791–2798.
42 M. J. Cuthbertson and P. H. Poole, *Phys. Rev. Lett.*, 2011, **106**, 115706.
43 J. C. Palmer, F. Martelli, Y. Liu, R. Car, A. Z. Panagiotopoulos and P. G. Debenedetti, *Nature*, 2014, **510**, 385–388.
44 J. C. Palmer, P. H. Poole, F. Sciortino and P. G. Debenedetti, *Chem. Rev.*, 2018, **118**, 9129–9151.
45 J. C. Palmer, A. Haji-Akbari, R. S. Singh, F. Martelli, R. Car, A. Z. Panagiotopoulos and P. G. Debenedetti, *J. Chem. Phys.*, 2018, **148**, 137101.
46 Y. Liu, A. Z. Panagiotopoulos and P. G. Debenedetti, *J. Chem. Phys.*, 2009, **131**, 104508.
47 D. Corradini, M. Rovere and P. Gallo, *J. Chem. Phys.*, 2010, **132**, 134508.
48 D. Paschek, *Phys. Rev. Lett.*, 2005, **94**, 217802.
49 M. Yamada, S. Mossa, H. E. Stanley and F. Sciortino, *Phys. Rev. Lett.*, 2002, **88**, 195701.
50 D. Paschek, A. Rüppert and A. Geiger, *ChemPhysChem*, 2008, **9**, 2737–2741.
51 J. L. Abascal and C. Vega, *J. Chem. Phys.*, 2005, **123**, 234505.
52 C. Vega and J. L. F. Abascal, *Phys. Chem. Chem. Phys.*, 2011, **13**, 19663–19688.
53 J. L. Abascal and C. Vega, *J. Chem. Phys.*, 2010, **133**, 234502.
54 J. W. Biddle, R. S. Singh, E. M. Sparano, F. Ricci, M. A. Gonzalez, C. Valeriani, J. L. Abascal, P. G. Debenedetti, M. A. Anisimov and F. Caupin, *J. Chem. Phys.*, 2017, **146**, 034502.
55 P. H. Handle and F. Sciortino, *J. Chem. Phys.*, 2018, **148**, 134505.
56 S. D. Overduin and G. N. Patey, *J. Chem. Phys.*, 2013, **138**, 184502.
57 S. D. Overduin and G. N. Patey, *J. Chem. Phys.*, 2015, **143**, 094504.
58 R. S. Singh, J. W. Biddle, P. G. Debenedetti and M. A. Anisimov, *J. Chem. Phys.*, 2016, **144**, 144504.
59 T. Sumi and H. Sekino, *RSC Adv.*, 2013, **3**, 12743–12750.
60 T. Yagasaki, M. Matsumoto and H. Tanaka, *Phys. Rev. E: Stat., Nonlinear, Soft Matter Phys.*, 2014, **89**, 020301.
61 K. T. Wikfeldt, A. Nilsson and L. G. M. Pettersson, *Phys. Chem. Chem. Phys.*, 2011, **13**, 19918–19924.
62 H. J. C. Berendsen, J. R. Grigera and T. P. Straatsma, *J. Phys. Chem.*, 1987, **91**, 6269–6271.
63 A. Scala, F. W. Starr, E. La Nave, H. E. Stanley and F. Sciortino, *Phys. Rev. E: Stat., Nonlinear, Soft Matter Phys.*, 2000, **62**, 8016.
64 F. Sciortino, E. La Nave and P. Tartaglia, *Phys. Rev. Lett.*, 2003, **91**, 155701.
65 A. Scala, F. W. Starr, E. La Nave, F. Sciortino and H. E. Stanley, *Nature*, 2000, **406**, 166.
66 W. L. Jorgensen, J. Chandrasekhar, J. D. Madura, R. W. Impey and M. L. Klein, *J. Chem. Phys.*, 1983, **79**, 926–935.
67 H. W. Horn, W. C. Swope, J. W. Pitera, J. D. Madura, T. J. Dick, G. L. Hura and T. Head-Gordon, *J. Chem. Phys.*, 2004, **120**, 9665–9678.
68 M. W. Mahoney and W. L. Jorgensen, *J. Chem. Phys.*, 2000, **112**, 8910–8922.
69 S. W. Rick, *J. Chem. Phys.*, 2004, **120**, 6085–6093.

70 O. Mishima and H. E. Stanley, *Nature*, 1998, **392**, 164–168.
71 O. Mishima, *J. Chem. Phys.*, 2010, **133**, 144503.
72 O. Mishima, *Phys. Rev. Lett.*, 2000, **85**, 334–336.
73 G. Franzese and H. E. Stanley, *J. Phys.: Condens. Matter*, 2007, **19**, 205126.
74 N. Giovambattista, in *Liquid polymorphism*, ed. H. E. Stanley, Wiley, Hoboken, NJ, 2013, vol. 103, pp. 113–138.
75 F. A. Gorelli, T. Bryk, M. Krisch, G. Ruocco, M. Santoro and T. Scopigno, *Sci. Rep.*, 2013, **3**, 1203.
76 P. F. McMillan and H. E. Stanley, *Nat. Phys.*, 2010, **6**, 479.
77 G. G. Simeoni, T. Bryk, F. A. Gorelli, M. Krisch, G. Ruocco, M. Santoro and T. Scopigno, *Nat. Phys.*, 2010, **6**, 503.
78 L. Xu, P. Kumar, S. V. Buldyrev, S.-H. Chen, P. H. Poole, F. Sciortino and H. E. Stanley, *Proc. Natl. Acad. Sci. U. S. A.*, 2005, **102**, 16558–16562.
79 F. W. Starr, F. Sciortino and H. E. Stanley, *Phys. Rev. E: Stat. Phys., Plasmas, Fluids, Relat. Interdiscip. Top.*, 1999, **60**, 6757.
80 G. Tammann and W. Hesse, *Z. Anorg. Allg. Chem.*, 1926, **156**, 245–257.
81 K. Ito, C. T. Moynihan and C. A. Angell, *Nature*, 1999, **398**, 492.
82 S. M. McClure, D. J. Safarik, T. M. Truskett and C. B. Mullins, *J. Phys. Chem. B*, 2006, **110**, 11033–11036.
83 K. Amann-Winkel, C. Gainaru, P. H. Handle, M. Seidl, H. Nelson, R. Bohmer and T. Loerting, *Proc. Natl. Acad. Sci. U. S. A.*, 2013, **110**, 17720–17725.
84 Y. Xu, N. G. Petrik, R. S. Smith, B. D. Kay and G. A. Kimmel, *Proc. Natl. Acad. Sci. U. S. A.*, 2016, **113**, 14921–14925.
85 K. H. Kim, A. Spah, H. Pathak, F. Perakis, D. Mariedahl, K. Amann-Winkel, J. A. Sellberg, J. H. Lee, S. Kim, J. Park, K. H. Nam, T. Katayama and A. Nilsson, *Science*, 2017, **358**, 1589–1593.
86 V. Holten, C. Qiu, E. Guillerm, M. Wilke, J. Rička, M. Frenz and F. Caupin, *J. Phys. Chem. Lett.*, 2017, **8**, 5519–5522.
87 F. Caupin, V. Holten, C. Qiu, E. Guillerm, M. Wilke, M. Frenz, J. Teixeira and A. K. Soper, *Science*, 2018, **360**, eaat1634.
88 K. H. Kim, A. Späh, H. Pathak, F. Perakis, D. Mariedahl, K. Amann-Winkel, J. A. Sellberg, J. H. Lee, S. Kim and J. Park, *et al.*, *Science*, 2018, **360**, eaat1729.
89 E. Mayer, *J. Appl. Phys.*, 1985, **58**, 663–667.
90 P. H. Handle and T. Loerting, *J. Chem. Phys.*, 2018, **148**, 124508.
91 O. Mishima, *J. Chem. Phys.*, 1994, **100**, 5910–5912.
92 O. Mishima, L. D. Calvert and E. Whalley, *Nature*, 1985, **314**, 76–78.
93 K. Winkel, M. S. Elsaesser, E. Mayer and T. Loerting, *J. Chem. Phys.*, 2008, **128**, 044510.
94 J. A. McMillan and S. C. Los, *Nature*, 1965, **206**, 806–807.
95 G. P. Johari, A. Hallbrucker and E. Mayer, *Nature*, 1987, **330**, 552–553.
96 A. Hallbrucker, E. Mayer and G. P. Johari, *J. Phys. Chem.*, 1989, **93**, 4986–4990.
97 A. Hallbrucker, E. Mayer and G. P. Johari, *Philos. Mag. B*, 1989, **60**, 179–187.
98 G. P. Johari, A. Hallbrucker and E. Mayer, *J. Chem. Phys.*, 1990, **92**, 6742–6746.
99 R. S. Smith and B. D. Kay, *Nature*, 1999, **398**, 788–791.
100 M. S. Elsaesser, K. Winkel, E. Mayer and T. Loerting, *Phys. Chem. Chem. Phys.*, 2010, **12**, 708–712.
101 O. Mishima, *J. Chem. Phys.*, 2004, **121**, 3161–3164.
102 M. Seidl, M. S. Elsaesser, K. Winkel, G. Zifferer, E. Mayer and T. Loerting, *Phys. Rev. B*, 2011, **83**, 100201.
103 P. H. Handle, M. Seidl and T. Loerting, *Phys. Rev. Lett.*, 2012, **108**, 225901.
104 J. N. Stern, M. Seidl-Nigsch and T. Loerting, *Proc. Natl. Acad. Sci. U. S. A.*, 2019, **116**, 9191–9196.
105 K. Amann-Winkel, R. Bohmer, F. Fujara, C. Gainaru, B. Geil and T. Loerting, *Rev. Mod. Phys.*, 2016, **88**, 20.
106 T. Loerting, V. Fuentes-Landete, P. H. Handle, M. Seidl, K. Amann-Winkel, C. Gainaru and R. Bohmer, *J. Non-Cryst. Solids*, 2015, **407**, 423–430.
107 K. Winkel, E. Mayer and T. Loerting, *J. Phys. Chem. B*, 2011, **115**, 14141–14148.
108 O. Mishima, *Nature*, 1996, **384**, 546–549.
109 O. Mishima, L. D. Calvert and E. Whalley, *Nature*, 1984, **310**, 393–395.
110 T. Loerting, K. Winkel, M. Seidl, M. Bauer, C. Mitterdorfer, P. H. Handle, C. G. Salzmann, E. Mayer, J. L. Finney and D. T. Bowron, *Phys. Chem. Chem. Phys.*, 2011, **13**, 8783–8794.
111 P. Brüggeller and E. Mayer, *Nature*, 1980, **288**, 569–571.
112 I. Kohl, L. Bachmann, A. Hallbrucker, E. Mayer and T. Loerting, *Phys. Chem. Chem. Phys.*, 2005, **7**, 3210–3220.
113 O. Mishima and Y. Suzuki, *J. Chem. Phys.*, 2001, **115**, 4199–4202.
114 N. Giovambattista, H. E. Stanley and F. Sciortino, *Phys. Rev. Lett.*, 2003, **91**, 115504.
115 J. Wong, D. A. Jahn and N. Giovambattista, *J. Chem. Phys.*, 2015, **143**, 074501.
116 N. Giovambattista, F. Sciortino, F. W. Starr and P. H. Poole, *J. Chem. Phys.*, 2016, **145**, 224501.
117 J. Engstler and N. Giovambattista, *J. Chem. Phys.*, 2017, **147**, 074505.
118 N. Giovambattista, F. W. Starr and P. H. Poole, *J. Chem. Phys.*, 2017, **147**, 044501.
119 P. H. Handle, F. Sciortino and N. Giovambattista, *J. Chem. Phys.*, 2019, **150**, 244506.
120 G. H. Meyer, M. B. Morrow, O. Wyss, T. E. Berg and J. L. Littlepage, *Science*, 1962, **138**, 1103–1104.
121 G. M. Marion, *Antarct. Sci.*, 1997, **9**, 92–99.
122 D. G. Archer and R. W. Carter, *J. Phys. Chem. B*, 2000, **104**, 8563–8584.
123 J. M. Borreguero and E. Mamontov, *J. Phys. Chem. B*, 2017, **121**, 4168–4173.
124 M. Oguni and C. A. Angell, *J. Chem. Phys.*, 1980, **73**, 1948–1954.
125 A. Chrétien, R. Kohlmuller and A. P. Rollet, *Nouveau traité de chimie minérale*, Masson et Cie, 1966.
126 C. A. Angell and E. J. Sare, *J. Chem. Phys.*, 1968, **49**, 4713–4714.
127 C. A. Angell and E. J. Sare, *J. Chem. Phys.*, 1970, **52**, 1058–1068.
128 C. Monnin, M. Dubois, N. Papaiconomou and J.-P. Simonin, *J. Chem. Eng. Data*, 2002, **47**, 1331–1336.

129 G. N. Ruiz, L. E. Bove, H. R. Corti and T. Loerting, *Phys. Chem. Chem. Phys.*, 2014, **16**, 18553–18562.
130 K. Hofer, A. Hallbrucker, E. Mayer and G. P. Johari, *J. Chem. Phys.*, 1989, **93**, 4674–4677.
131 Y. Suzuki and O. Mishima, *Phys. Rev. Lett.*, 2000, **85**, 1322–1325.
132 H. Kanno, *J. Phys. Chem.*, 1987, **91**, 1967–1971.
133 Y. Suzuki and O. Mishima, *J. Chem. Phys.*, 2002, **117**, 1673–1676.
134 Y. Suzuki and O. Mishima, *J. Chem. Phys.*, 2013, **138**, 084507.
135 Y. Suzuki and Y. Tominaga, *J. Chem. Phys.*, 2011, **134**, 244511.
136 L. E. Bove, S. Klotz, J. Philippe and A. M. Saitta, *Phys. Rev. Lett.*, 2011, **106**, 125701.
137 T. Loerting, C. G. Salzmann, K. Winkel and E. Mayer, *Phys. Chem. Chem. Phys.*, 2006, **8**, 2810–2818.
138 S. Y. Hsich, P. B. Macedo, C. J. Montrose and R. W. Gammon, *J. Chem. Phys.*, 1972, **56**, 1663–1669.
139 C. A. Angell, E. J. Sare, J. Donnella and D. R. MacFarlane, *J. Phys. Chem.*, 1981, **85**, 1461–1464.
140 H. Kanno, K. Shimada and K. Katoh, *Chem. Phys. Lett.*, 1983, **103**, 219–221.
141 D. R. MacFarlane, R. K. Kadiyala and C. A. Angell, *J. Phys. Chem.*, 1983, **87**, 235–238.
142 D. R. Macfarlane, R. K. Kadiyala and C. A. Angell, *J. Chem. Phys.*, 1983, **79**, 3921–3927.
143 D. R. Macfarlane, R. K. Kadlyala and C. A. Angell, *J. Phys. Chem.*, 1983, **87**, 1094–1095.
144 D. Corradini and P. Gallo, *J. Phys. Chem. B*, 2011, **115**, 14161–14166.
145 D. Corradini, P. Gallo and M. Rovere, *J. Chem. Phys.*, 2008, **128**, 244508.
146 D. Corradini, P. Gallo and M. Rovere, *J. Chem. Phys.*, 2009, **130**, 154511.
147 D. Corradini, P. Gallo and M. Rovere, *J. Phys.: Condens. Matter*, 2010, **22**, 284104.
148 P. Gallo, D. Corradini and M. Rovere, *J. Chem. Phys.*, 2013, **139**, 204503.
149 L. E. Bove, C. Dreyfus, R. Torre and R. M. Pick, *J. Chem. Phys.*, 2013, **139**, 044501.
150 D. R. MacFarlane, J. Scheirer and S. I. Smedley, *J. Phys. Chem.*, 1986, **90**, 2168–2173.
151 O. Mishima, *J. Chem. Phys.*, 2005, **123**, 154506.
152 O. Mishima, *J. Chem. Phys.*, 2007, **126**, 244507.
153 R. Leberman and A. K. Soper, *Nature*, 1995, **378**, 364–366.
154 E. Williams and C. A. Angell, *J. Phys. Chem.*, 1977, **81**, 232–237.
155 B. Prével, J. F. Jal, J. Dupuy-Philon and A. K. Soper, *J. Chem. Phys.*, 1995, **103**, 1886–1896.
156 H. R. Corti, F. J. Nores-Pondal and C. A. Angell, *Phys. Chem. Chem. Phys.*, 2011, **13**, 19741–19748.
157 G. Bullock and V. Molinero, *Faraday Discuss.*, 2014, **167**, 371.
158 G. N. Ruiz, K. Amann-Winkel, L. E. Bove, H. R. Corti and T. Loerting, *Phys. Chem. Chem. Phys.*, 2018, **20**, 6401–6408.
159 N. Giovambattista, T. Loerting, B. R. Lukanov and F. W. Starr, *Sci. Rep.*, 2012, **2**, 390.
160 L. Le and V. Molinero, *J. Phys. Chem. A*, 2011, **115**, 5900–5907.
161 O. Mishima, *J. Phys. Chem. B*, 2011, **115**, 14064–14067.
162 Y. Suzuki and O. Mishima, *J. Phys.: Condens. Matter*, 2009, **21**, 155105.
163 K. Winkel, M. Bauer, E. Mayer, M. Seidl, M. S. Elsaesser and T. Loerting, *J. Phys.: Condens. Matter*, 2008, **20**, 494212.
164 T. Loerting, W. Schustereder, K. Winkel, C. G. Salzmann, I. Kohl and E. Mayer, *Phys. Rev. Lett.*, 2006, **96**, 025702.
165 P. H. Handle and T. Loerting, *Phys. Rev. B*, 2016, **93**, 064204.
166 J. Chiu, F. W. Starr and N. Giovambattista, *J. Chem. Phys.*, 2013, **139**, 184504.
167 J. Chiu, F. W. Starr and N. Giovambattista, *J. Chem. Phys.*, 2014, **140**, 114504.
168 P. H. Handle and T. Loerting, *J. Chem. Phys.*, 2018, **148**, 124509.
169 D. Corradini, M. Rovere and P. Gallo, *J. Phys. Chem. B*, 2011, **115**, 1461–1468.
170 R. Souda, *J. Chem. Phys.*, 2006, **125**, 181103.
171 J. Holzmann, R. Ludwig, A. Geiger and D. Paschek, *Angew. Chem., Int. Ed.*, 2007, **46**, 8907–8911.
172 E. Mamontov, *J. Phys. Chem. B*, 2009, **113**, 14073–14078.
173 M. E. Gallina, L. Bove, C. Dreyfus, A. Polian, B. Bonello, R. Cucini, A. Taschin, R. Torre and R. M. Pick, *J. Chem. Phys.*, 2009, **131**, 124504.
174 S. C. Santucci, L. Comez, F. Scarponi, G. Monaco, R. Verbeni, J.-F. Legrand, C. Masciovecchio, A. Gessini and D. Fioretto, *J. Chem. Phys.*, 2009, **131**, 154507.
175 E. Mamontov, A. Faraone, E. W. Hagaman, K. S. Han and E. Fratini, *J. Phys. Chem. B*, 2010, **114**, 16737–16743.
176 D. A. Turton, C. Corsaro, D. F. Martin, F. Mallamace and K. Wynne, *Phys. Chem. Chem. Phys.*, 2012, **14**, 8067–8073.
177 M. Nakanishi, P. Griffin, E. Mamontov and A. P. Sokolov, *J. Chem. Phys.*, 2012, **136**, 124512.
178 E. Mamontov and M. Ohl, *Phys. Chem. Chem. Phys.*, 2013, **15**, 10732–10739.
179 C. Corsaro, D. Mallamace, N. Cicero, S. Vasi, G. Dugo and F. Mallamace, *Physica A*, 2016, **442**, 261–267.
180 S. Schneider and M. Vogel, *J. Chem. Phys.*, 2018, **149**, 104501.
181 M. P. Longinotti, M. A. Carignano, I. Szleifer and H. R. Corti, *J. Chem. Phys.*, 2011, **134**, 244510.
182 S. W. Rick, *J. Chem. Phys.*, 2004, **120**, 6085–6093.
183 I. Gladich, P. Shepson, I. Szleifer and M. A. Carignano, *Chem. Phys. Lett.*, 2010, **489**, 113–117.
184 I. S. Joung and T. E. Cheatham, *J. Phys. Chem. B*, 2008, **112**, 9020–9041.
185 M. Patra and M. Karttunen, *J. Comput. Chem.*, 2004, **25**, 678–689.
186 P. Auffinger, T. E. Cheatham and A. C. Vaiana, *J. Chem. Theory Comput.*, 2007, **3**, 1851–1859.
187 J. L. Aragones, M. Rovere, C. Vega and P. Gallo, *J. Phys. Chem. B*, 2014, **118**, 7680–7691.

188 J. W. Biddle, V. Holten and M. A. Anisimov, *J. Chem. Phys.*, 2014, **141**, 074504.
189 V. Holten and M. A. Anisimov, *Sci. Rep.*, 2012, **2**, 713.
190 C. A. Angell and R. D. Bressel, *J. Phys. Chem.*, 1972, **76**, 3244–3253.
191 C. A. Angell and J. C. Tucker, *J. Phys. Chem.*, 1980, **84**, 268–272.
192 H. Kanno, R. J. Speedy and C. A. Angell, *Science*, 1975, **189**, 880–881.
193 H. Kanno and C. A. Angell, *J. Phys. Chem.*, 1977, **81**, 2639–2643.
194 K. Miyata, H. Kanno, T. Niino and K. Tomizawa, *Chem. Phys. Lett.*, 2002, **354**, 51–55.
195 K. Hofer, G. Astl, E. Mayer and G. P. Johari, *J. Phys. Chem.*, 1991, **95**, 10777–10781.
196 M. Gordon and J. S. Taylor, *J. Appl. Chem.*, 1952, **2**, 493–500.
197 E. Mayer, *J. Phys. Chem.*, 1986, **90**, 4455–4461.
198 G. Fleissner, A. Hallbrucker and E. Mayer, *J. Phys. Chem.*, 1993, **97**, 4806–4814.
199 G. Fleissner, A. Hallbrucker and E. Mayer, *Chem. Phys. Lett.*, 1994, **218**, 93–99.
200 G. Fleissner, A. Hallbrucker and E. Mayer, *J. Phys. Chem.*, 1995, **99**, 8401–8404.
201 G. Fleissner, A. Hallbrucker and E. Mayer, *J. Phys. Chem. B*, 1998, **102**, 6239–6247.
202 M. Mitterböck, G. Fleissner, A. Hallbrucker and E. Mayer, *J. Phys. Chem. B*, 1999, **103**, 8016–8025.
203 Z. Zhao and C. A. Angell, *Angew. Chem., Int. Ed.*, 2016, **55**, 2474–2477.
204 T. Koop, B. Luo, A. Tsias and T. Peter, *Nature*, 2000, **406**, 611–614.
205 B. Zobrist, U. Weers and T. Koop, *J. Chem. Phys.*, 2003, **118**, 10254–10261.
206 S. Woutersen, B. Ensing, M. Hilbers, Z. Zhao and C. A. Angell, *Science*, 2018, **359**, 1127–1131.
207 Glycerine Producer's Association (New York), *Nothing Takes the Place of Glycerine: 1583 Ways To Use It*, Soap and Detergent Association, New York, 1949.
208 C. Polge, A. U. Smith and A. S. Parkes, *Nature*, 1949, **164**, 666.
209 P. R. Davis-Searles, A. J. Saunders, D. A. Erie, D. J. Winzor and G. J. Pielak, *Annu. Rev. Biophys. Biomol. Struct.*, 2001, **30**, 271–306.
210 J. G. Baust, D. Gao and J. M. Baust, *Organogenesis*, 2009, **5**, 90–96.
211 G. D. Elliott, S. Wang and B. J. Fuller, *Cryobiology*, 2017, **76**, 74–91.
212 M. P. Buera, Y. Roos, H. Levine, L. Slade, H. R. Corti, D. S. Reid, T. Auffret and C. A. Angell, *Pure Appl. Chem.*, 2011, **83**, 1567–1617.
213 M. Paglario and M. Rossi, *The Future of Glycerol*, Royal Society of Chemistry, Cambridge, 2010.
214 J. A. Padró, L. Saiz and E. Guàrdia, *J. Mol. Struct.*, 1997, **416**, 243–248.
215 L. B. Lane, *Ind. Eng. Chem.*, 1925, **17**, 924.
216 A. Puzenko, Y. Hayashi, Y. E. Ryabov, I. Balin, Y. Feldman, U. Kaatze and R. Behrends, *J. Phys. Chem. B*, 2005, **109**, 6031–6035.
217 Y. Hayashi, A. Puzenko and Y. Feldman, *J. Non-Cryst. Solids*, 2006, **352**, 4696–4703.
218 D. Harran, *Bull. Soc. Chim. Fr.*, 1978, I40–I44.
219 S. Ablett, M. J. Izzard and P. J. Lillford, *J. Chem. Soc., Faraday Trans.*, 1992, **88**, 789–794.
220 S. Sudo, M. Shimomura, N. Shinyashiki and S. Yagihara, *J. Non-Cryst. Solids*, 2002, **307–310**, 356–363.
221 A. Inaba and O. Andersson, *Thermochim. Acta*, 2007, **461**, 44–49.
222 I. Popov, A. Greenbaum Gutina, A. P. Sokolov and Y. Feldman, *Phys. Chem. Chem. Phys.*, 2015, **17**, 18063–18071.
223 L. S. Zhao, Z. X. Cao and Q. Wang, *Sci. Rep.*, 2015, **5**, 15714.
224 J. Bachler, V. Fuentes-Landete, D. A. Jahn, J. Wong, N. Giovambattista and T. Loerting, *Phys. Chem. Chem. Phys.*, 2016, **18**, 11058–11068.
225 Y. Hayashi, A. Puzenko, I. Balin, Y. E. Ryabov and Y. Feldman, *J. Phys. Chem. B*, 2005, **109**, 9174–9177.
226 A. Inaba, N. Sakisato, A. K. Bickerstaffe and S. M. Clarke, *J. Neutron Res.*, 2005, **13**, 87–90.
227 A. Inaba, *Pure Appl. Chem.*, 2006, **78**, 1025–1037.
228 O. D. C. Palacios, A. Inaba and O. Andersson, *Thermochim. Acta*, 2010, **500**, 106–110.
229 K. Murata and H. Tanaka, *Nat. Mater.*, 2012, **11**, 436–443.
230 Y. Suzuki and O. Mishima, *J. Chem. Phys.*, 2014, **141**, 094505.
231 A. Angell, *Nat. Mater.*, 2012, **11**, 362–364.
232 K. Murata and H. Tanaka, *Nat. Commun.*, 2013, **4**, 2844.
233 J. R. Bruijn, T. H. van der Loop and S. Woutersen, *J. Phys. Chem. Lett.*, 2016, **7**, 795–799.
234 R. Kurita and H. Tanaka, *Phys. Rev. B*, 2006, **73**, 104202.
235 W. Hage, A. Hallbrucker, E. Mayer and G. P. Johari, *J. Chem. Phys.*, 1994, **100**, 2743–2747.
236 M. Avrami, *J. Chem. Phys.*, 1939, **7**, 1103–1112.
237 M. Avrami, *J. Chem. Phys.*, 1940, **8**, 212–224.
238 M. Avrami, *J. Chem. Phys.*, 1941, **9**, 177–184.
239 J. Mosses, C. D. Syme and K. Wynne, *J. Phys. Chem. Lett.*, 2015, **6**, 38–43.
240 C. D. Syme, J. Mosses, M. Gonzalez-Jimenez, O. Shebanova, F. Walton and K. Wynne, *Sci. Rep.*, 2017, **7**, 42439.
241 M. Tarnacka, O. Madejczyk, M. Dulski, P. Maksym, K. Kaminski and M. Paluch, *J. Phys. Chem. C*, 2017, **121**, 19442–19450.
242 J. E. K. Schawe, *Thermochim. Acta*, 2006, **451**, 115–125.
243 A. Bogdan, M. J. Molina, H. Tenhu and T. Loerting, *J. Phys. Chem. A*, 2015, **119**, 4515–4523.
244 Y. Suzuki, *J. Chem. Phys.*, 2018, **149**, 204501.
245 E. Whalley, D. D. Klug and Y. P. Handa, *Nature*, 1989, **342**, 782–783.
246 Y. Suzuki and O. Mishima, *J. Chem. Phys.*, 2016, **145**, 024501.
247 S. H. Chen, L. Liu, E. Fratini, P. Baglioni, A. Faraone and E. Mamontov, *Proc. Natl. Acad. Sci. U. S. A.*, 2006, **103**, 9012–9016.
248 C. U. Kim, M. W. Tate and S. M. Gruner, *Proc. Natl. Acad. Sci. U. S. A.*, 2011, **108**, 20897–20901.
249 F. Mallamace, P. Baglioni, C. Corsaro, S. H. Chen, D. Mallamace, C. Vasi and H. E. Stanley, *J. Chem. Phys.*, 2014, **141**, 165104.

250 F. Mallamace, C. Corsaro, P. Baglioni, E. Fratini and S. H. Chen, *J. Phys.: Condens. Matter*, 2012, **24**, 064103.
251 J. R. Authelin, A. P. MacKenzie, D. H. Rasmussen and E. Y. Shalaev, *J. Pharm. Sci.*, 2014, **103**, 2663–2672.
252 F. Mallamace, C. Corsaro, D. Mallamace, C. Vasi, S. Vasi and H. E. Stanley, *J. Chem. Phys.*, 2016, **144**, 064506.
253 D. A. Jahn, J. Wong, J. Bachler, T. Loerting and N. Giovambattista, *Phys. Chem. Chem. Phys.*, 2016, **18**, 11042–11057.
254 Y. Suzuki, *J. Chem. Phys.*, 2017, **147**, 064511.
255 M. Seidl, K. Amann-Winkel, P. H. Handle, G. Zifferer and T. Loerting, *Phys. Rev. B*, 2013, **88**, 289.
256 M. Seidl, A. Fayter, J. N. Stern, G. Zifferer and T. Loerting, *Phys. Rev. B*, 2015, **91**, 144201.
257 C. G. Salzmann, T. Loerting, I. Kohl, E. Mayer and A. Hallbrucker, *J. Phys. Chem. B*, 2002, **106**, 5587–5590.
258 J. Engstler and N. Giovambattista, *J. Phys. Chem. B*, 2018, **122**, 8908–8920.
259 F. O. Akinkunmi, D. A. Jahn and N. Giovambattista, *J. Phys. Chem. B*, 2015, **119**, 6250–6261.
260 J. L. Finney, A. Hallbrucker, I. Kohl, A. K. Soper and D. T. Bowron, *Phys. Rev. Lett.*, 2002, **88**, 225503.
261 D. T. Bowron, J. L. Finney, A. Hallbrucker, I. Kohl, T. Loerting, E. Mayer and A. K. Soper, *J. Chem. Phys.*, 2006, **125**, 194502.
262 T. Loerting and N. Giovambattista, *J. Phys.: Condens. Matter*, 2006, **18**, R919–R977.
263 J. Blieck, F. Affouard, P. Bordat, A. Lerbret and M. Descamps, *Chem. Phys.*, 2005, **317**, 253–257.
264 Y. Marcus, *Phys. Chem. Chem. Phys.*, 2000, **2**, 4891–4896.
265 K. Takamura, H. Fischer and N. R. Morrow, *J. Pet. Sci. Eng.*, 2012, **98–99**, 50–60.
266 B. Chen, E. E. Sigmund and W. P. Halperin, *Phys. Rev. Lett.*, 2006, **96**, 145502.
267 G. Blond and D. Simatos, *Thermochim. Acta*, 1991, **175**, 239–247.
268 K. Elamin, J. Sjostrom, H. Jansson and J. Swenson, *J. Chem. Phys.*, 2012, **136**, 104508.
269 J. L. Green and C. A. Angell, *J. Phys. Chem.*, 1989, **93**, 2880–2882.
270 N. Karger and H. D. Ludemann, *Z. Naturforsch., C: J. Biosci.*, 1991, **46**, 313–317.
271 S. S. N. Murthy and G. Singh, *Thermochim. Acta*, 2008, **469**, 116–119.
272 A. Nagoe and M. Oguni, *J. Phys.: Condens. Matter*, 2010, **22**, 325103.
273 H. Kanno, K. Miyata, K. Tomizawa and H. Tanaka, *J. Phys. Chem. A*, 2004, **108**, 6079–6082.
274 D. Corradini, Z. Su, H. E. Stanley and P. Gallo, *J. Chem. Phys.*, 2012, **137**, 184503.
275 W. L. Jorgensen, D. S. Maxwell and J. Tirado-Rives, *J. Am. Chem. Soc.*, 1996, **118**, 11225–11236.
276 G. Wada and S. Umeda, *Bull. Chem. Soc. Jpn.*, 1962, **35**, 646–652.
277 C. U. Kim, B. Barstow, M. W. Tate and S. M. Gruner, *Proc. Natl. Acad. Sci. U. S. A.*, 2009, **106**, 4596–4600.
278 C. U. Kim, Y. F. Chen, M. W. Tate and S. M. Gruner, *J. Appl. Crystallogr.*, 2008, **41**, 1–7.
279 C. U. Kim, Q. Hao and S. M. Gruner, *Acta Crystallogr., Sect. D: Biol. Crystallogr.*, 2006, **62**, 687–694.
280 C. U. Kim, R. Kapfer and S. M. Gruner, *Acta Crystallogr., Sect. D: Biol. Crystallogr.*, 2005, **61**, 881–890.
281 C. U. Kim, M. W. Tate and S. M. Gruner, *Proc. Natl. Acad. Sci. U. S. A.*, 2015, **112**, 11765–11770.
282 S. Kriminski, C. L. Caylor, M. C. Nonato, K. D. Finkelstein and R. E. Thorne, *Acta Crystallogr., Sect. D: Biol. Crystallogr.*, 2002, **58**, 459–471.
283 D. H. Juers and B. W. Matthews, *Q. Rev. Biophys.*, 2004, **37**, 105–119.
284 D. Ringe and G. A. Petsko, *Biophys. Chem.*, 2003, **105**, 667–680.
285 H. E. Stanley, P. Kumar, S. Han, M. G. Mazza, K. Stokely, S. V. Buldyrev, G. Franzese, F. Mallamace and L. Xu, *J. Phys.: Condens. Matter*, 2009, **21**, 504105.
286 S. Lemke, P. H. Handle, L. J. Plaga, J. N. Stern, M. Seidl, V. Fuentes-Landete, K. Amann-Winkel, K. W. Köster, C. Gainaru, T. Loerting and R. Böhmer, *J. Chem. Phys.*, 2017, **147**, 034506.
287 D. Vitkup, D. Ringe, G. A. Petsko and M. Karplus, *Nat. Struct. Biol.*, 2000, **7**, 34–38.
288 M. Tarek and D. J. Tobias, *Phys. Rev. Lett.*, 2002, **88**, 138101.
289 A. L. Tournier, J. Xu and J. C. Smith, *Biophys. J.*, 2003, **85**, 1871–1875.
290 C. M. Tonauer, M. Seidl-Nigsch and T. Loerting, *J. Phys.: Condens. Matter*, 2018, **30**, 034002.
291 O. Mishima, K. Takemura and K. Aoki, *Science*, 1991, **254**, 406–408.
292 V. Molinero and E. B. Moore, *J. Phys. Chem. B*, 2009, **113**, 4008–4016.
293 F. H. Stillinger and T. A. Weber, *Phys. Rev. B*, 1985, **31**, 5262–5271.
294 D. T. Limmer and D. Chandler, *J. Chem. Phys.*, 2011, **135**, 134503.
295 E. B. Moore and V. Molinero, *Nature*, 2011, **479**, 506–508.
296 E. B. Moore and V. Molinero, *J. Chem. Phys.*, 2010, **132**, 244504.
297 D. T. Limmer and D. Chandler, *Proc. Natl. Acad. Sci. U. S. A.*, 2014, **111**, 9413–9418.
298 S. V. Buldyrev, G. Franzese, N. Giovambattista, G. Malescio, M. R. Sadr-Lahijany, A. Scala, A. Skibinsky and H. E. Stanley, *Physica A*, 2002, **304**, 23–42.
299 S. V. Buldyrev, G. Malescio, C. A. Angell, N. Giovambattista, S. Prestipino, F. Saija, H. E. Stanley and L. Xu, *J. Phys.: Condens. Matter*, 2009, **21**, 504106.
300 E. A. Jagla, *J. Chem. Phys.*, 1999, **111**, 8980–8986.
301 E. A. Jagla, *Phys. Rev. E*, 2001, **63**, 061501.
302 G. Franzese, *J. Mol. Liq.*, 2007, **136**, 267–273.
303 J. Luo, L. Xu, E. Lascaris, H. E. Stanley and S. V. Buldyrev, *Phys. Rev. Lett.*, 2014, **112**, 135701.
304 A. B. d. Oliveira, P. A. Netz, T. Colla and M. C. Barbosa, *J. Chem. Phys.*, 2006, **124**, 084505.
305 J. Y. Luo, L. M. Xu, C. A. Angell, H. E. Stanley and S. V. Buldyrev, *J. Chem. Phys.*, 2015, **142**, 224501.

306 L. Xu, S. V. Buldyrev, N. Giovambattista, C. Angell and H. E. Stanley, *J. Chem. Phys.*, 2009, **130**, 054505.
307 J. Y. Abraham, S. V. Buldyrev and N. Giovambattista, *J. Phys. Chem. B*, 2011, **115**, 14229–14239.
308 A. Gordon and N. Giovambattista, *Phys. Rev. Lett.*, 2014, **112**, 145701.
309 S. Reisman and N. Giovambattista, *J. Chem. Phys.*, 2013, **138**, 064509.
310 S. V. Buldyrev, P. Kumar, P. G. Debenedetti, P. J. Rossky and H. E. Stanley, *Proc. Natl. Acad. Sci. U. S. A.*, 2007, **104**, 20177–20182.
311 K. Lum, D. Chandler and J. D. Weeks, *J. Phys. Chem. B*, 1999, **103**, 4570–4577.
312 D. Corradini, S. V. Buldyrev, P. Gallo and H. E. Stanley, *Phys. Rev. E*, 2010, **81**, 061504.
313 D. Corradini, P. Gallo, S. V. Buldyrev and H. E. Stanley, *Phys. Rev. E*, 2012, **85**, 051503.
314 H. M. Gibson and N. B. Wilding, *Phys. Rev. E*, 2006, **74**, 019903.
315 C. A. Cerdeiriña and P. G. Debenedetti, *J. Chem. Phys.*, 2016, **144**, 164501.
316 S. Chatterjee and P. G. Debenedetti, *J. Chem. Phys.*, 2006, **124**, 154503.
317 H. Laksmono, T. A. McQueen, J. A. Sellberg, N. D. Loh, C. Huang, D. Schlesinger, R. G. Sierra, C. Y. Hampton, D. Nordlund, M. Beye, A. V. Martin, A. Barty, M. M. Seibert, M. Messerschmidt, G. J. Williams, S. Boutet, K. Amann-Winkel, T. Loerting, L. G. Pettersson, M. J. Bogan and A. Nilsson, *J. Phys. Chem. Lett.*, 2015, **6**, 2826–2832.
318 M. D. Ediger and P. Harrowell, *J. Chem. Phys.*, 2012, **137**, 080901.
319 M. Zanatta, L. Tavagnacco, E. Buratti, M. Bertoldo, F. Natali, E. Chiessi, A. Orecchini and E. Zaccarelli, *Sci. Adv.*, 2018, **4**, eaat5895.
320 E. W. Roddenberry, in *Star Trek*, 1966.